This is to certify that the
thesis entitled

TECHNIQUES FOR ENHANCING IMPACT TESTING

presented by

Brandon Geoffrey Gulker

has been accepted towards fulfillment
of the requirements for the

M.S. degree in Mechanical Engineering

Major Professor's Signature

12/17/2009

Date

TECHNIQUES FOR ENHANCING IMPACT TESTING

By

Brandon Geoffrey Gulker

A THESIS

Submitted to
Michigan State University
In partial fulfillment of the requirements
for the degree of

MASTER OF SCIENCE

Mechanical Engineering

2009

ABSTRACT

TECHNIQUES FOR ENHANCING IMPACT TESTING

By

Brandon Geoffrey Gulker

Impact events occur frequently during the life cycle of most structures. This thesis presents three enhancements to impact testing. (1) A full-field displacement measurement technique called Projection Moiré was implemented for impact testing which provided the out-of-plane displacement of plate specimens during impact loading. This measurement revealed the initiation and growth of major delamination in the plate. Additionally, the measurements were compared to measurements made at a single point by a load cell. (2) Since material properties may be different under dynamic loading than under static loading, it is desirable to establish an efficient test method to extract the dynamic material properties. The Virtual Fields Method was explored for use in impact testing. Simulated plate bending from Finite Element Analysis was used to determine the ideal test setup. Methods for using the Projection Moiré data for real experiments were then explored and a methodology for future study proposed. (3) In order to observe the internal damage as a function of time, translucent specimens were manufactured. Methods for implementing Projection Moiré measurements at the same time as viewing the internal damage were explored. It was demonstrated that this simultaneous measurement was possible.

To my parents, who have taught me

more than could be put in writing.

ACKNOWLEDGEMENTS

I am extremely grateful for the assistance and support of my academic advisor, Dr. Dahsin Liu. Without him, this work would not have been possible.

Additionally, I am grateful for the participation of Dr. Soonsung Hong and Dr. Alfred Loos in my defense committee.

The financial support from the U.S. Army TARDEC, Warren, MI was greatly appreciated.

Finally, I would like to thank my colleagues, past and present, who have provided assistance both professionally and personally: Guojing Li, Liangkai Ma, Tao Jia, Anupam Dhyani, Shawn Klann, and Kirit Rosario.

TABLE OF CONTENTS

LIST OF TABLES

LIST OF FIGURES

KEY TO SYMBOLS AND ABBREVIATIONS

α	=	Indentation
γ	=	Acceleration
ε	=	Strain
θ	=	Grating projection angle
ρ	=	Density
σ	=	Stress
ν	=	Poisson's Ratio
Φ	=	Phase
A	=	Background intensity
B	=	Background modulation
CL	=	Clamped
d	=	Marker paint diameter
D	=	Bending stiffness
DWIT	=	Drop-weight impact tester
E	=	Young's Modulus
f	=	Body force
f_0	=	Carrier frequency
FTP	=	Fourier Transform Profilometry
h	=	Camera position
k	=	Curvature
K	=	Power Law fitting constant
L	=	Specimen length

n	=	Power Law fitting constant
r^2	=	Correlation
R	=	Impactor radius
S_f	=	Surface
SS	=	Simply supported
T	=	Traction
u	=	Displacement
U	=	Energy
V	=	Volume
w	=	Out-of-plane displacement

Chapter 1: Introduction

Abstract

A major difficulty in using composite materials in real structures is their performance under impact loads. A wide variety of real loading scenarios are under dynamic conditions, and the damage process under these scenarios is still not well understood. Several techniques have been established to objectively characterize a materials impact performance and to compare different materials. However, these studies have primarily been based on analyzing the data obtained from a load cell. Load cell data is a measurement of only a single point of the specimen. Some studies have utilized high speed camera technology to observe the surface response. This thesis explores techniques which can be used to enhance impact study. Full-field displacement was implemented for impact testing. A methodology for obtaining material properties from this data was established. Additionally, translucent glass/epoxy composite materials were used to observe the internal damage progression during impact loading.

1.1 Literature review

Composite materials provide an advantage over conventional materials such as metals in that their stiffness to weight ratios are much higher. For this reason, they have become popular in applications where weight reduction is a priority, such as in the aerospace industry. In spite of their advantages, composites have a disadvantage in that they are not as well understood. The

damage processes present within the material are quite complex. This is especially true for dynamic loading conditions.

There are a wide variety of dynamic loads that present themselves in the life-cycle of any product. For an airplane, for example, impact loads range from the relatively low velocities of a repair tool being dropped onto a panel to the relatively high velocities of a collision with a bird. Each impact event has the potential damage the composite material and thus degrade its performance.

In order to properly design a structure using composite materials and take into consideration these and other loading scenarios, it is necessary to properly understand the damage process occurring within the composite structure. For this reason, a number of experimental studies have been carried out. A considerable amount of work has been done in an attempt to properly characterize the impact performance of various composite structures.

A large number of studies have been conducted concerning the behavior of composite materials under impact loading. Reviews of the research can be found in several locations such as the book by Abrate [1.1] and the paper by Richardson and Wiseheard [1.2]. Several techniques have been developed to assist in the characterization and comparison of different composite materials.

Basic methods for comparing the performance of various composite materials under impact loading involve impacting several different materials using the same impacting mass and velocity. Their force-time and force-deflection plots can be compared and any differences can indicate a materials performance. In addition to comparing the curves, several quantities can be

calculated and compared. For example, the energy absorbed by the composite (absorbed energy), the force at which a change in stiffness was observed (critical force), deflection at which a change in stiffness was observed (critical deflection), the maximum deflection, and the maximum force have all been used in the comparison of composite materials [1.2].

Pilchak et al. [1.3] used this approach in comparing laminated composite materials with angles of 0-90 degrees between layers. In addition, different methods of stitching layers together were compared. With this method it was possible to establish that, in general, small angles provided a higher degree of impact resistance than large angles. Additionally, it was found that stitching layers together increased the impact resistance.

Rosario [1.4] compared different methods of weaving layers together by comparing the absorbed energy, the force history, and images obtained from a high speed camera. He was able characterize the strengths and weaknesses of different weaving methods and identify which composite structure provided the highest impact resistance. By comparing these results with the high speed camera images, the highest impact resistance was identified as being due to the high degree of fiber straining in the rear layer of the composite. The composites with the highest impact resistance had a plateau in the force history at the peak force. This plateau corresponded to images where the rear layer had a significant degree of delamination. The delamination of the rear layer could be seen to the naked eye whereas the internal delamination was not visible. This

study established the importance of the rear layer in designing composite materials for impact resistance.

More advanced techniques for comparing composite materials have also been established. Liu [1.5] developed the energy profiling method. In this method, different composite specimens of the same material and orientation are impacted with incrementally increasing amounts of energy. The amount of energy absorbed by the composite (absorbed energy) is plotted versus the incident kinetic energy of the impacting mass (impact energy) for the entire set of data. Also, the load-deflection plots for each specimen are then plotted on the same graph to create a portrait of the materials impact resistance and damage progression. This energy profiling method was used to identify key impact performance parameters of composite plates such as the penetration and perforation thresholds as well as the range of penetration process. Dominant damage modes were also identified for different ranges of impact energy. The dominant damage modes, were cited as indentation, matrix cracking/crushing, delamination, lamina splitting, bending fractures, and fiber breakage. This tool provided a method with which to compare two composite materials.

Feraboli and Kedward [1.6] developed another method to compare composite materials. In their study, several quantities were defined from the data. One was the coefficient of restitution which is the ratio of the exit to impact velocity of the impacting mass. It was observed that when this quantity was plotted as a function of the kinetic energy of the impacting mass, several kinks were present in the plot. These kinks divided the behavior at different impact

energies into different regions. At what impact energy these kinks were present provided a gage of the material's impact damage resistance. Plotting the total contact duration as a function of the impacting energy confirmed the significance of these regions. A second impact was performed on the damaged specimens in order to asses and compare the residual performance of the materials. This technique could be advantageous in comparing multiple material configurations. In a later paper [1.7], the same authors used this method to compare the results from tests with square fixtures to tests with circular fixtures. It was found that there was no significant variation between the results with the various fixtures.

Delamination is the primary damage mode which introduces a degradation in the material stiffness. Several studies have been conducted in which the initiation of delamination was investigated. Many researchers have observed an point in the loading portion of the force-time curve for which major oscillations initiate [1.7, 1.8, 1.9]. This oscillation has been attributed to an initiation of delamination. Since it was not possible to observe the delamination initiation and growth within the composite, this served as the only means of identifying the delamination. Schoeppner and Abrate [1.8] theorized that the oscillations after delamination and initiation were due to crack initiation, arrest, reload, and propagation cycles. They could not, however, observe the phenomenon directly.

In addition to the study of damage processes, it has been observed that composite materials can exhibit a strain-rate dependence. For some materials, the material properties under dynamic loading may be different than those at static loading. Lee and Liu [1.10] demonstrated that glass/epoxy composite

material present different behavior when loaded statically versus dynamically. This was shown by performing static and dynamic indentation tests on thick glass/epoxy laminates by supporting them rigidly at the base. It was observed that, for the same peak force, the maximum indentation for the static loading was higher than that of the dynamic loading. Gulker [1.11] also observed a difference between the static and dynamic response during dynamic indentation. However, it was observed that the response for all of the dynamic testing was the same, regardless of impact velocity (impact velocities ranging from 0.94 m/s to 2.64 m/s were explored). This suggests that properties governing dynamic response differ from those governing static response. However, there is very little, if any, variation in properties as the impact velocity is changed within a small range. A discussion of this subject can be found in Appendix A of this thesis.

1.2 Motivation

The previous work has largely focused on analyzing data obtained from a load cell at the point of impact. Although this has been useful, it is limited by the fact that the measurements are only recorded at a single point. With this approach, conclusions concerning the materials response beyond this point can only be made indirectly. Since a large amount of the damage processes occur beyond the impact point, studies could be greatly enhanced by making measurements of the full specimen.

Some work has been done to include the observations from a high speed camera. This provides a means of observing the response of the rear surface of the specimen during the impact event. Since the plates under analysis are thin

relative to the other dimensions, observing a single surface is an acceptable choice. Even though the surface behavior can be observed with this technique, not measurements are directly taken here. The study would be greatly enhanced if some objective values for the strains or displacements were obtained.

From the previous techniques, a useful area to focus future study is in the implementation of a means of measuring the rear surface. There have been some dynamic studies using full-field measurements (see Chapter 2 for a discussion), but more work needs to be done to establish a reliable methodology. The present work implements Projection Moiré to measure the out-of-plane displacements of the rear surface of the specimen. It is then possible to objectively discuss the material response during the impact loading.

Once the full-field displacements are obtained, it is desirable to use this data to obtain the material properties of the specimen. It has already been established that the dynamic material properties may differ from the static properties. Chapter 3 of this thesis focuses on this subject. A technique called the Virtual Fields Method is explored and a methodology for implementing this technique in drop-weight impact tests is established.

Although the full-field displacement measurements provide a significant addition to the impact testing, it is still only possible to measure a single surface's behavior. Since much of the damage is inside of the composite, in order to be able to fully characterize the damage process, it is necessary to observe how this internal damage progresses. This would be possible if the specimen were translucent. With glass/epoxy composites, it is possible to make the specimen

translucent if the index of refraction of the fiber and the matrix are similar. Chapter 4 of this thesis explores the use of translucent specimens in impact testing. The specimen was viewed with a high speed camera and the evolution of the internal damage was observed. To enhance this study, techniques for simultaneously implementing Projection Moiré along with the translucent specimen were explored.

1.3 Objectives

The simplicity of the drop-weight impact tester has led to its frequent use in impact studies as demonstrated in the literature review. Since it is a test that is performed frequently, it is desirable that experimental techniques be developed that maximize the amount of information that can be obtained from this setup. Most studies in the literature investigate measurements only at a single point, the impact point. It would be advantageous to make measurements over the entire surface of the impacted plate. One of the objectives of this thesis was to identify and implement a full-field measurement technique to measure the plate response. It was also desired that the rear surface measurements made here be compared to the single point measurements on the impacting surface.

Once the full-field response was obtained, it was desired to use this information as thoroughly as possible. Since delamination causes a localized change in bending stiffness, it should present a discontinuity in the slope of the out-of-plane displacement. For this reason, it should be possible to observe the initiation and growth of major delamination within the specimen by observing the

change in the specimen displacement. One of the goals of this thesis was to identify this trend.

An additional way to use the full-field data is to obtain the bending stiffnesses of the plate. A method exists (the Virtual Fields Method discussed in Chapter 3) for identifying material properties from the full field response of the specimen. Identifying an acceptable methodology for implementing this method was an objective of this thesis.

In addition to exploring the surface response of the specimen, it was desired to observe the internal damage growth. This could be done through the use of translucent composites, as discussed in Chapter 4. It was desired to measure the surface response and the internal damage growth simultaneously. The objective was to implement a technique which allowed for both measurements.

1.4 Approaches

Projection Moiré was chosen to be the full-field measurement method to be used in this study. In this technique, a grating is projected onto the specimen surface, and the out-of-plane displacement can be obtained from the shift in the projected grating as the specimen deforms. Contour plots for all time were compared and displacement profiles along a line through the point of impact were drawn in order to identify trends. This made it possible to identify the localized change in bending stiffness due to major delamination, and thus identify its initiation and growth.

In the attempt to identify methods for finding the bending stiffnesses from the impact test, it was desired that alternative sets of boundary conditions to the standard set (clamped on four edges) be explored. The response for different boundary conditions is reliant on different bending stiffnesses. In order to accurately identify each property, it is necessary that the response be dependent on each of them. For this reason, it is possible that the optimum set of boundary conditions is different from those typically used. In order to explore different cases, a finite element model was built using Abaqus to simulate the deflection which would be present in static testing of these plates. It was assumed that the trends present in this test would be similar to the elastic portion of the impact response. The technique of using simulated data instead of experimental data allowed for an efficient exploration of many different combinations of boundary conditions. The optimal boundary conditions were identified and the implementation of this technique for real experiments was explored.

In order to measure both the internal damage and the out-of-plane displacement, it was necessary that the translucent composites reflect enough light back to the camera so that the projected grating can be accurately captured. Several techniques were explored. One technique was to coat half of the specimen with matte white paint to obtain a completely opaque half and a translucent half. Since the material and boundary conditions were symmetric, the behavior of each half could be assumed to be representative of the other half. In order to measure both quantities for the full-field, a balance between transparency and opacity was obtained by coating the surface of the translucent

specimen with semi-transparent paint. Both woven and laminated composites were investigated. It was possible to obtain an estimate of the crack speed by recording the amount of growth between frames of the high speed camera.

1.5 Organization of thesis

In Chapter 2 of this thesis, the implementation of full-field methods is explored. First, a literature review of several alternative techniques is presented, and the reason for choosing Projection Moiré is presented. A summary of the theory behind the method is presented and the experimental implementation is outlined. An accuracy study was implemented to validate the experimental setup. Results for plate impact tests are then presented. The observations concerning the initiation and growth of major delamination are presented. The displacement, velocity, and acceleration at the impact point for the rear and impact surfaces is presented and compared.

Chapter 3 of the thesis explores the implementation of the Virtual Fields Method in impact testing. A brief summary of the theory is presented and a review of its past applications is conducted. The techniques used in the present work are then explained. The results from the simulated data obtained from finite element analysis are then presented, and the ideal setup for future testing is identified. The implementation of this method for real experiments is explored and developed. Reasons for the poor experimental results are discussed, and a more rigorous technique for extending the method to impact testing is proposed.

Chapter 4 of this thesis explores the use of translucent composites for observing the internal damage growth during the impact event. The methods for

measuring the damage growth and the out-of-plane displacement simultaneously are presented. Contour plots of the displacement are presented along with the delamination growth. The delamination growth is also compared to the force history. An estimation of the crack speed with time is then presented.

Chapter 5 of this thesis summarizes the conclusions made from the previous work. It also presents an outline of the future work that should be conducted.

1.6 References

[1.1] Abrate, S. Impact on Composite Structures. 1998, New York, NY: Cambridge University Press.

[1.2] Richardson, M.O.W., and Wisheart, M.J., "Review of low-velocity impact properties of composite materials" *Composites: Part A*, Vol. 27A, 1996, pp. 1123-1131.

[1.3] Pilchak, A.L., Uchiyama, T., and Liu, D. "Low-Velocity Impact Response of Small-Angle Laminated Composites," *AIAA Journal*. Vol. 44, 2006, pp. 3080-3087.

[1.4] Rosario, K, "Quasi-three-dimensional woven composites," Master's Thesis, Michigan State University, East Lansing, MI, 2008.

[1.5] Liu, D, "Characterization of Impact Properties and Damage Process of Glass/Epoxy Composite Laminates," *Journal of Composite Materials*, Vol. 38, 2004, 1425-1442.

[1.6] Feraboli, P, and Kedward, KT "Enhanced Evaluation of the Low-Velocity Impact Response of Composite Plates," *AIAA Journal,* Vol 42, 2004, 2143-2152.

[1.7] Feraboli, P, and Kedward, KT, "A new composite structure impact performance assessment program," *Composites Science and Technology*, 2006, Vol 66, 1336-1347.

[1.8] Schoeppner, GA, and Abrate, S "Delamination threshold loads for low velocity impact on composite laminates," *Composites: Part A,* Vol 31, 2000, 903-915.

[1.9] Belingardi, G, and Vadori, R, "Low velocity impact tests of laminate glass-fiber-epoxy matrix composite material plates," *International Journal of Impact Engineering*, 2002, Vol 27, 213-229.

[1.10] Lee, C-Y, and Liu, D "Effect of impact velocity on the indentation of thick composite laminate," *Experimental Techniques,* 2008.

[1.11] Gulker, B, "Experimental Methods for Impact of Composite Materials," 2009, Proceedings of the SEM Annual Conference, Paper no. 575.

Chapter 2: Impact testing with Projection Moiré

Abstract

There have been a large number of studies conducted for impact testing of materials. Most of the analysis done in the past has been focused on using the force measurement from a load cell. Calculating the displacement from this measurement requires the data to be integrated twice with respect to time. Since this is an indirect approach, it is desirable to establish a way to directly measure the displacement during the impact event. Additionally, if it is possible to measure the displacement of the entire surface rather than just a single point, it should be possible to better characterize the damage process in materials. There are a range of full-field displacement measurement methods. Projection Moiré was selected as the full-field displacement measurement method to be used for this study. It was selected due to several factors: quality of results in the literature, simplicity of its setup, and availability of a program to process the images. The method has been applied to impact testing of laminated composite materials using a drop-weight impact tester (DWIT). The displacement of the rear surface was plotted and the delamination initiation and propagation was visible in the results. The Projection Moiré results were then compared to the single point measurements of the impacting surface using a load cell. Good correlation was seen between the measurements of the two surfaces.

2.1 Introduction

There are several works in the literature concerning the application of optical methods to dynamic measurements. Kokidko et al. [2.1] used the Shadow Moiré method to study the deformation of a composite specimen under ballistic loading. Chai et al. [2.2] also used the Shadow Moiré method but for low-velocity compression studies of composite materials. An advantage of the Shadow Moiré method is that it is very well established and easy to implement. Unfortunately, however, the test setup requires the placement of a reference grating very near the specimen (typically less than 15 mm away). This would result in the destruction of a grating any time the maximum displacement was as large or greater than this gap. This would both be cost prohibitive as well as make it impossible to study the displacement history after the grating was destroyed.

One of the most common optical methods found in the literature is Digital Image Correlation (DIC). A review of the method has been presented by Sutton et al. [2.3]. In this method, a pattern is placed on the specimen and the deformation of that pattern is recorded and related to the displacement. Reu et al. [2.4] used the method to measure the rear surface deformation of a steel plate during impact testing. Tiwari et al. [2.5] studied the deformation of an aluminum plate under explosive loading. This method is beneficial because both the in-plane and out-of-plane deformations can be directly measured. A disadvantage of this method, however, is that it requires the use of two cameras to record out-

of-plane deformation. This increases the cost of implementation and the complexity of the experimental setup.

Fourier Transform Profilometry (FTP) is a method similar to Projection Moiré in that a grating system is also projected onto the specimen. A review of the method has been written by Su and Chen [2.6]. The difference is in the way this information is processed. In FTP, the displacement calculation can be extracted from a single image rather than several phase shifted images. This advantage has led several researchers to pursue it for dynamic studies. Zhang et al. [2.7] used the method to study the rotation of fan blades. Su et al. [2.8] used it to study the topography of the surface of a can of paint while it was being stirred. Zhang and Su [2.9] studied a drum vibration using FTP. Paepegem et al. [2.10] used FTP to study the out-of-plane deformation of a composite panel subjected to a bird strike. For the study of the deformation during bird strike, the resulting displacement contours were very noisy. The method needs further refinement to increase its usefulness.

Projection Moiré using phase shifting has also been used for dynamic studies. Since phase shifting in its traditional form requires actual physical shifting of a grating and recording several images, it has been limited in its application to static studies. If a grating has to be physically shifted and several images recorded, these images cannot be at exactly the same time. This severely limits the speed at which this method can be implemented. Pan and Huang [2.11] introduce a method in which several phase shifted gratings are embedded in a single image by using a different color for each phase shift. The

individual phase shifts could later be extracted digitally. A disadvantage of this method is that it would be sensitive to the color of the image and the light intensity distribution on the object's surface. Additionally, many high speed cameras on the market currently are black and white only, thus eliminating this as an option.

Chan and Bryanston-Cross [2.12] showed how Projection Moiré methods involving phase stepping were less computationally intensive than FTP. They also introduced a phase estimating method which was faster than FTP by about ten times for high resolution images and four times for low resolution images. Since it is desired to implement an optical displacement measurement method in dynamic testing using a high speed camera, there may be several hundred images to process. The increase in computational efficiency is quite attractive for this reason. Heredia and Patterson refined the Projection Moiré method and made it much more user friendly by developing the JOSHUA software package to automate the displacement calculation from a reference and object image [2.13]. This software package used a similar phase estimating approach as Chan and Bryanston-Cross' method [2.12]. In their study, the method and software were validated by running a series of tests on numerically simulated data and images of static objects. Heredia and Patterson [2.13] studied the accuracy of the method by experimentally measuring cone shapes and inclined plates. Measurements for these tests were reported to be within 1% of the measurement range.

2.2 Methods

2.2.1 Drop weight impact tester

The device used in this study to create the dynamic loading was the Dynatup drop-weight impact tester, model 8250. In this setup, a freely falling weight falls through some prescribed distance and impacts the specimen. The drop height determines the velocity at which the impact event will occur. The various components of this device are shown in the figure below. The actual device is shown in Figure 2.4.

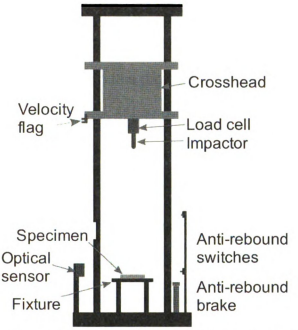

Figure 2.1. Schematic of the DWIT machine. The actual device is shown in Figure 2.4.

The impactor used in this study had a hemispherical nose with a diameter of 12.7 mm (0.5 in). The rebound brake is used in this device to prevent the impactor from impacting the specimen more than one time. If the mass rebounds

from the specimen, the brake is activated and prevents any additional impact events. The optical sensor serves two purposes. The first is to trigger the data acquisition system and the second is to record the initial velocity. The initial velocity is calculated based on two flags which pass through the sensor immediately prior to impact of the specimen. The load cell and optical sensor are connected to the data acquisition system. The DWIT data acquisition system was calibrated at the beginning of this study. The procedure can be found in Appendix A of this thesis.

2.2.2 Projection Moiré theory

Projection Moiré measurements were used in this study to measure full field out-of-plane displacements. In this method, a system of lines (grating) is projected at some angle, θ, onto the object to be measured. Typically, the object is viewed normal to the specimen. An image is captured before and after deformation. From these images, it is possible to extract the phase data which is directly related to the out-of-plane displacement. By subtracting the phase of the reference image from the deformed image, the phase difference is obtained. The phase difference is related to the deformation between the two frames. The basic principles of the method are presented in this section. A comprehensive discussion of the method can be found in the literature such as the paper by Heredia and Patterson [2.13].

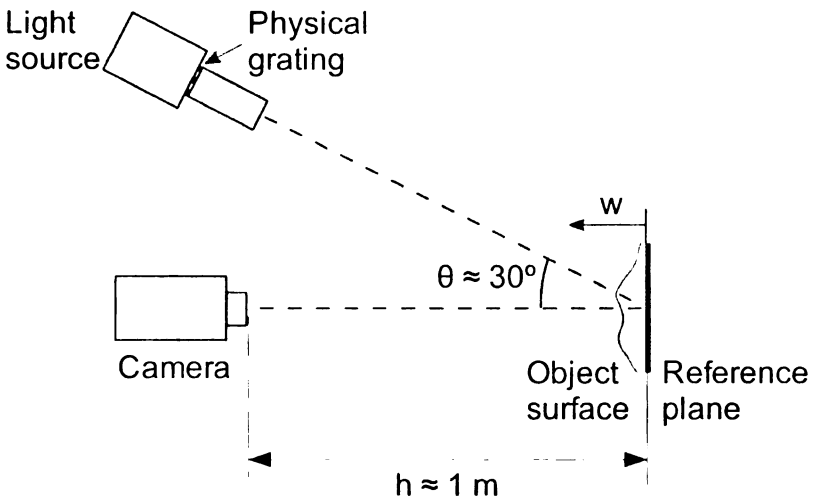

Figure 2.2. Schematic showing the general setup for Projection Moiré measurements.

From the above test setup, the intensity of the recorded image can be expressed by the following equation.

$$I(x,y)=A(x,y)+B(x,y)\cos\left[2\pi f_0 x+\Phi(x,y)\right] \tag{2.1}$$

A and B represent the background intensity and modulation. The term f_0 is called the carrier frequency which is related to the grating pitch. Φ is the phase and $\Delta\Phi$ is the difference between the deformed and undeformed phase which is related to displacement of the specimen. The phase, Φ, is obtained by obtaining several intensity maps and solving the system of equations for the phase. The additional intensity maps are found by virtually shifting the grating as discussed in [2.13]. Since phase is a discontinuous quantity, it must be unwrapped to obtain a continuous quantity in space.

If the phase for the deformed object and a flat reference object are both obtained, then the subtraction of these two terms provides the displacement of the deformed object. If the grating and the camera are sufficiently far away from

the object (infinite optics assumption), the displacement is related to the phase by the following equation.

$$w = \frac{p}{2\pi \tan\theta} \Delta\Phi \tag{2.2}$$

In the above equation, w is the out-of-plane displacement, p is the pitch of the projected grating, and θ is the angle between the viewing axis and the projection axis. The infinite optics assumption can be used as long as the distance from the camera to the object surface, h, is at least one order of magnitude larger than the object being studied. In this study, the specimen was 75 mm along the edge, so the distance must be at least 750 mm.

A program called JOSHUA has been developed by Heredia and Patterson to perform the above Projection Moiré calculations for a pair of images [2.13]. This study has made extensive use of this tool (JOSHUA version 1.12.2).

2.2.3 Projection Moiré setup

For the DWIT (discussed in Chapter 2 of this thesis), Projection Moiré was implemented as shown in the following schematic.

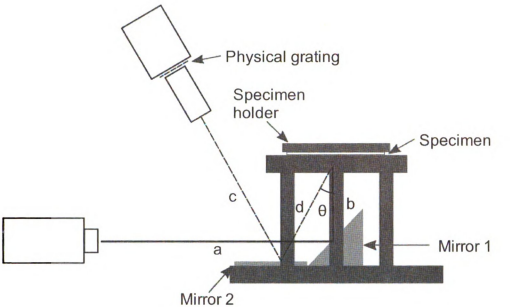

Figure 2.3. Schematic of how the Projection Moiré method was applied to the DWIT test setup. In the setup for this testing, a+b ≈ 750 mm, c+d ≈ 750 mm, and θ ≈ 30°.

The specimen is positioned such that the fiber direction of the rear layer is perpendicular to the direction of the projected grating lines. This ensures that matrix cracking will not be confused with the grating lines. The actual DWIT machine and the Projection Moiré components are presented in the following figure.

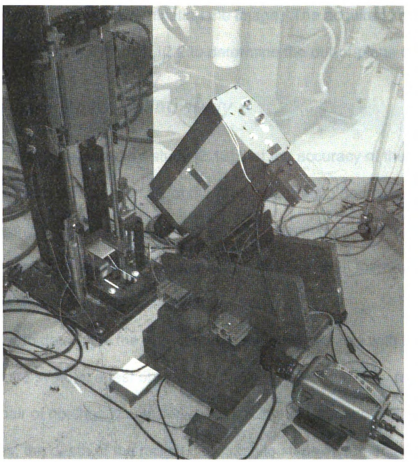

Figure 2.4. Projection Moiré method applied to the DWIT setup

The images were recorded with a Phantom v12 high speed camera from Vision Research. The speed of the images was 7000-15000 frames/sec depending on the test. Considering that an average impact event for this loading scenario lasts about 10 ms, this frame rate provided an adequate number of data points. Since the light sensitivity of high speed cameras decreases as the frame rate increases, the rear surface of the specimen was coated with a white matte paint to maximize the amount of light reflected to the camera, and therefore maximize the frame rate which could be used in the experiments. Additionally, all of the fixture components were painted with a black matte paint to prevent any

undesired reflections from contaminating the image. The acquired images were then processed using JOSHUA 1.12.2 to determine the out-of-plane deformation.

2.2.4 Projection Moiré grating study

It is known from Heredia's study [2.13] that the accuracy of the Projection Moiré method increases as the size of the projected grating decreases. However, the minimum projected grating allowed for using this method is limited by the resolution of the camera. If the grating is too fine, then there will not be enough pixels to properly represent each grating line.

In order to determine the appropriate grating size for use with the Projection Moiré system, a test object was developed with carefully machined notches. A pair of notches was milled into a 0.5 in thick aluminum plate. Along these notches, the depth of the milling increased in steps incrementally. Initially, the depth was such that the mill barely scratched the surface. This was defined as the zero reference for the rest of the steps. When the mill had traveled laterally for 10.16 mm (0.4 in), the milling depth was increased by 0.025 mm (0.001 in). This was repeated until the edge of the plate was reached. The process was then repeated for the second notch. The schematic of the stepping increments is shown below.

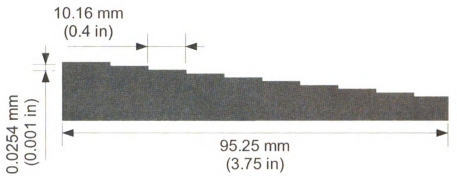

Figure 2.5. Schematic of the milling steps taken for one notch of the machine aluminum plate.

The actual machined plate is shown in the following image.

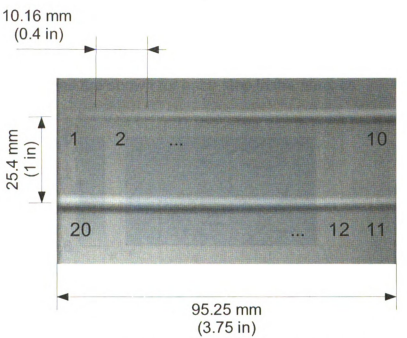

Figure 2.6. Image of the calibration plate. Notches were milled from an aluminum plate at incremental depths.

As shown in Figure 2.2, the camera was positioned about 750 mm from the test object and the projection angle, θ was about 30°. Three different physical gratings were used. They were 10, 20 and 30 lines/mm Ronchi Rulings purchased from Edmund Optics. The lens system used to focus the physical

gratings onto the specimen also magnified the gratings so that they covered the entire surface of the specimen. The sizes of the projected gratings on the specimen plane were 0.54, 0.94, and 1.08 lines/mm, respectively. The increment between the second and third gratings was smaller since increasing it any further resulted in the camera not being able to distinguish between lines. The resolution of the camera during this test was 1024 x 1280 pixels. As a result of the camera resolution, each pair of lines of the projected grating was represented by 11.74, 6.91, and 5.82 pixels, respectively. These values were calculated by counting the number of grating lines in the image and then dividing that number by the resolution of the image. The Projection Moiré results for each grating are shown below. Profiles are shown for each step in the notches.

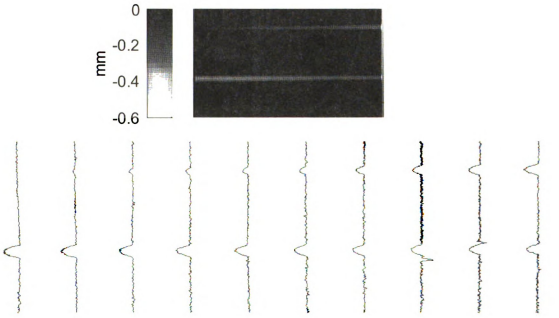

Figure 2.7. Displacement contour and profiles for the projected grating of 0.54 lines/mm.

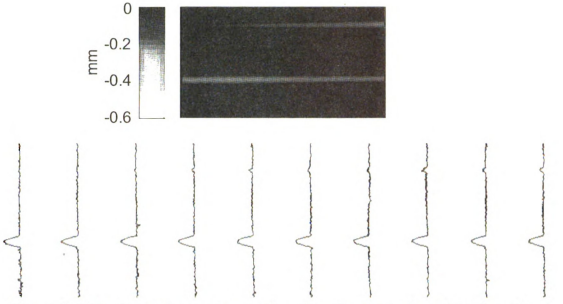

Figure 2.8.Displacement contour and profiles for the projected grating of 0.94 lines/mm.

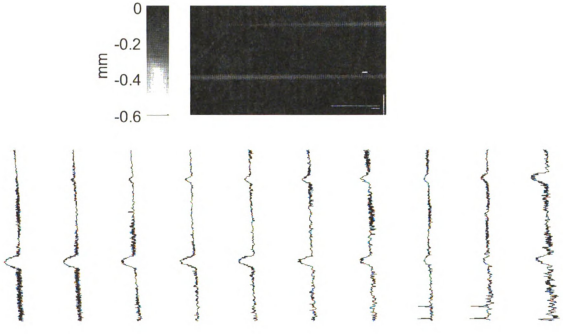

Figure 2.9. Displacement contour and profiles for the projected grating of 1.08 lines/mm.

The depth of each step was plotted for each grating and is shown in the following figure.

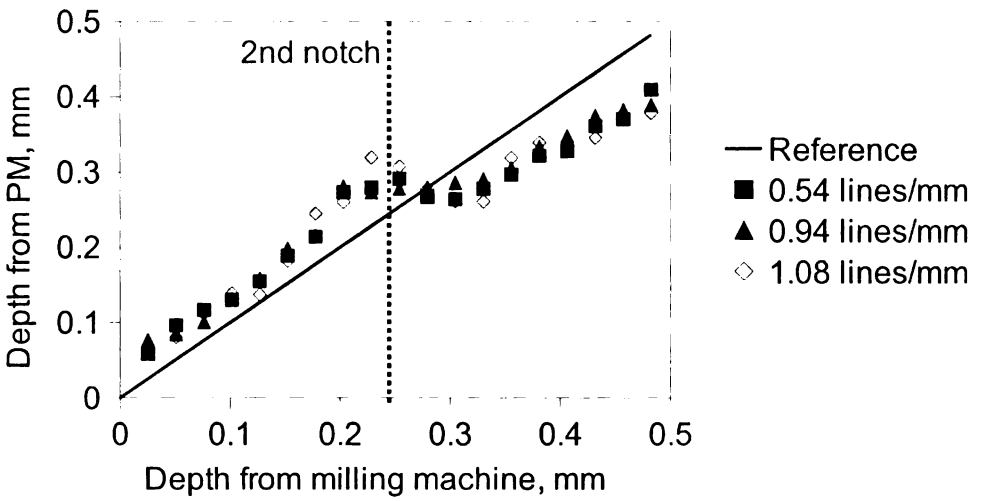

Figure 2.10. Comparison between the prescribed depth from the milling process and the depth measured from Projection Moiré.

The largest deviation from the prescribed depth for any of the measurements in the graph above was 0.103 mm. The mean deviation for the 0.54, 0.94, and 1.08 lines/mm data sets was 0.049, 0.044, and 0.052 mm, respectively. The accuracy of the milling machine was 0.025 mm (0.001 inch), so some of this deviation can be attributed to machining errors. At the location of the dashed line, it is seen that the Projection Moiré results all exhibit a bend. It is believed that this bend is due to the completion of the first notch and the initiation of the second notch. The results for 0.54 and 0.94 lines/mm are closer to the prescribed depth than that of the 1.08 lines/mm case indicating that once the projected grating becomes too fine, accuracy decreases.

An increase in the amount of noise present is seen as the grating becomes too fine. To quantify this effect, the standard deviation of the calculated displacement in the flat regions of the plate was calculated.

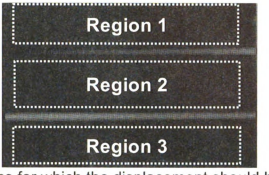

Figure 2.11. Regions for which the displacement should be zero.

Table 2.1. Comparison of the standard deviation of the displacement measured from Projection Moiré which should have zero values.

		Standard Deviation
Physical grating: 10 lines/mm Projected grating: 11.74 px/line-pair	Region 1	0.0389
	Region 2	0.0313
	Region 3	0.0302
	All regions	**0.0324**
Physical grating: 20 lines/mm Projected grating: 6.91 px/line-pair	Region 1	0.0199
	Region 2	0.0189
	Region 3	0.0236
	All regions	**0.0214**
Physical grating: 30 lines/mm Projected grating: 5.82 px/line-pair	Region 1	0.0423
	Region 2	0.0529
	Region 3	0.0842
	All regions	**0.0765**

From the above study, the deviation was the lowest when there were 6.91 pixels per line-pair. It was concluded that this case should be used in subsequent tests as the minimum for the combination of grating density and camera resolution.

Selection of the grating frequency depends on the camera resolution for a given

test. If a finer grating density is desired, then a higher camera resolution will be required in order to satisfy this requirement.

2.3 Results and discussion

2.3.1 Full-field displacement of the rear surface

A square 125 mm x125 mm composite laminate which was clamped along all four edges such that a specimen testing area 75 mm x 75 mm was visible. Clamping was applied by two clearance holes in the specimen on each edge outside of the testing area. Two steel plates sandwiched the composite specimen by bolting the assembly together through these clearance holes as shown in Figure 2.8.

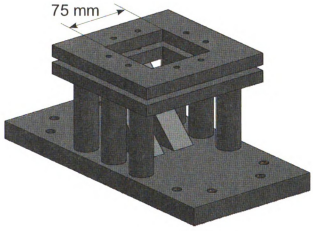

Figure 2.12. The standard fixture used in the DWIT testing. The specimen was bolted to ensure clamped boundary conditions were obtained.

The specimen was impacted at the center of this region. The impacting mass fell from a height of 320 mm with a mass of 5.16 kg. The force history was recorded by the load cell and the rear surface deflection was recorded by the Projection

Moiré system at a frame rate of 15,000 frames/sec. The time duration between each frame of the high speed camera was 0.067 ms. The total impact duration for this test was approximately 7 ms, so the impact event was represented by about 100 images. Below, 18 evenly spaced images are shown to represent the deformation history. The full frame rate of the camera was not used in this figure since there were so many frames. The time step between each frame shown in this figure is 0.4 ms.

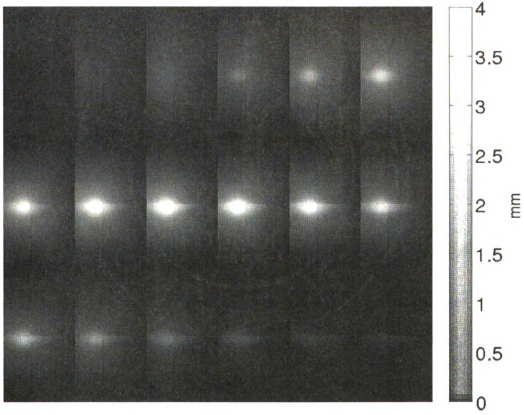

Figure 2.13 Contours for evenly spaced time steps during the impact event. The time step between each image is 0.4 ms.

Profile lines through the impact point are dawn as shown below.

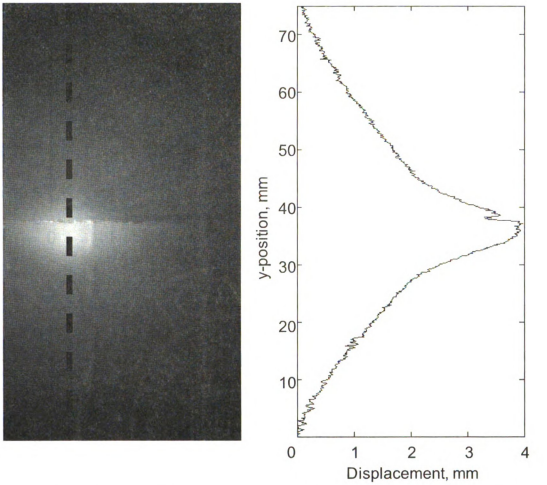

Figure 2.14. Contour image (left) and displacement profile (right) along the dotted line through the impact point.

Curves similar to the ones in the figure above were drawn for different time steps to show how the displacement changes with time. This was done for both the loading and unloading histories.

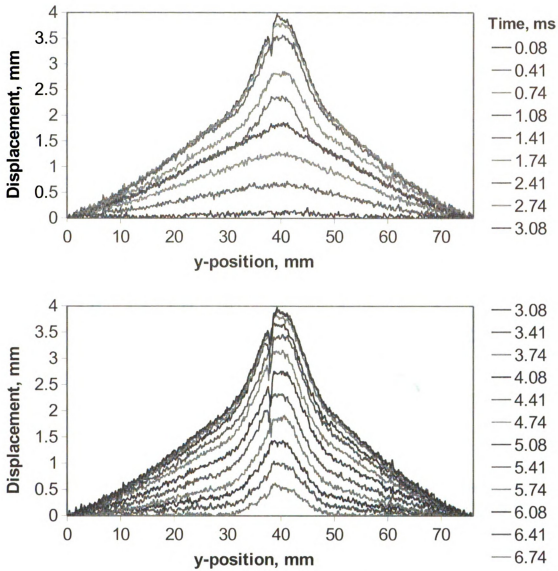

Figure 2.15. Profile lines drawn for loading (top) and unloading (bottom) histories. The time step between each image is 0.33 ms.

It is seen that deformations early in the loading history is such that the profile looks very much like a triangle. At some point, however, the triangular region stops growing for a period of time and a small protruded region develops. After this turning point in the deformation behavior, both the triangular and protruded regions continue to grow for the remainder of the loading history. Upon unloading, the protruded region stops growing any further and both regions

decrease in their degree of deformation. There is some amount of permanent deformation in the protruded region due to delamination.

The profiles through the impact point are compared with the force history in the plot below.

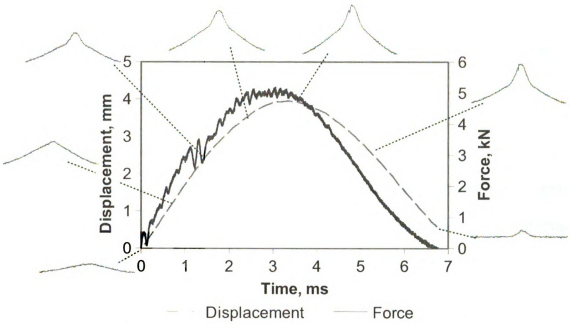

Figure 2.16. The force history from the impacting surface and the impact point displacement from the rear surface. Displacement profile lines are shown for various times.

It is seen in this image how the delamination grows compared to the force history. The initiation of major delamination is seen as a disturbance in the force-time curve. Also, once the maximum force has been reached, the size of the delaminated region ceases to grow any further.

It is seen from the above discussion that the material response to impact loading is more fully understood when the Projection Moiré measurements are included in the study. Since the damage process is one of the major criteria when comparing two or more composite structures, this tool could be utilized in

future work in order to more objectively and fully compare them. The significance of this method is further demonstrated when Rosario's [2.14] results are taken into consideration. In his study, the rear layer was identified as one of the primary factors in determining how much energy was absorbed by a composite plate under impact loading. If a similar study were conducted using Projection Moiré measurements, the materials could be better characterized and compared.

2.3.2 Comparison with the single point method

The results from the Projection Moiré from the rear surface at the point of impact were compared with the measurements of the load cell from the impacting surface at the location of impact. The load cell provides a measurement of force which can be related to the acceleration by Newton's Second Law if the impacting mass is rigid. Integration of this data provides the velocity, and a second integration provides the displacement. The rear surface and the impacting surface displacements are compared in the following figure.

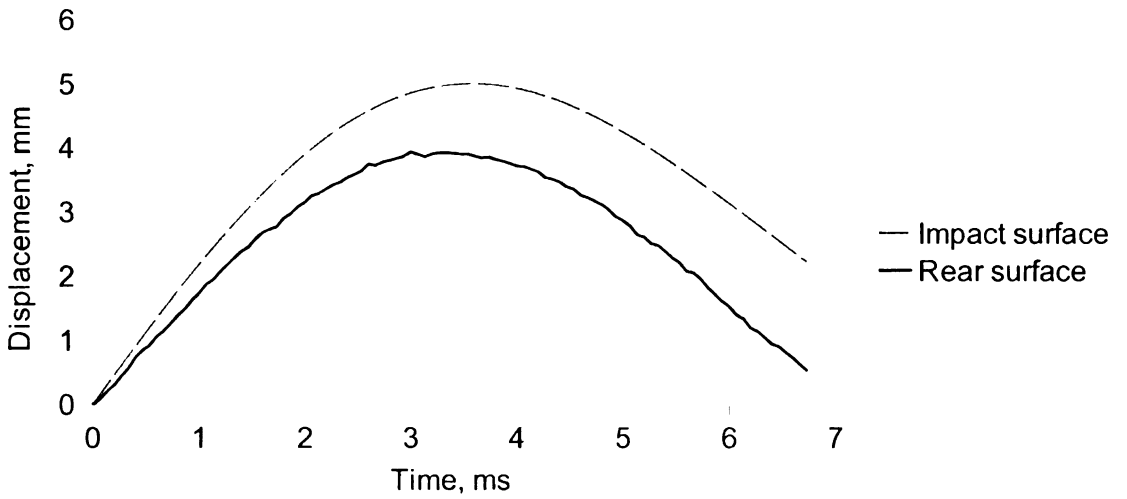

Figure 2.17. Comparison of the displacement of the impact surface and rear surface at the point of impact.

There is a difference in the magnitude between the impact surface an the rear surface. The peaks differ by a magnitude of 0.94 mm, and the final displacement differs by a magnitude of 0.78 mm. Neither of the surface displacements return to zero due to permanent damage that occurs during the impact event. The impact surface suffers from some permanent amount of indentation from the impactor. The rear surface suffers from delamination. A study of the dynamic and static indentation performance of a 25.4 mm (1 in) thick composite plate rigidly supported on its rear face was conducted previously [2.15]. The peak force was related to the maximum indentation during the loading. It is known that in the present test, the maximum force was 5 kN. In the case of the 25.4 mm thick composite, this corresponded to a maximum indentation of about 0.25 mm. Although the thickness and the stacking sequence of the composite in this test is different from that of the previous work, it expected that the indentation for the present case is at least in the same order of magnitude as before. Indentation

would would take place on the impact surface only, so this would account for some of the difference between the values. Since the measurements were taken on opposite surfaces of the specimen, and it is known that indentation will create a difference between the results for each measurement, it was concluded that the results were acceptable.

Since the rear surface displacement history is known, it is possible to calculate the velocity and acceleration histories by differentiating the data. Since differentiation is sensitive to noise, it was necessary to first smooth the data with respect to time. A polynomial was fit to the displacement history from Projection Moiré by the Least Squares Method. Selecting a low degree polynomial provides a poorer fit to the data, but is more smooth. Selecting a high degree polynomial provides a more accurate representation of the original curve, but is less smooth since the original curve contains noise. In order to obtain an acceptable fit, a balance must be found between these two extremes. From past experience, a fifth order polynomial was selected. The displacement history at the impact point of the rear surface with the corresponding polynomial fit is shown in the following figure.

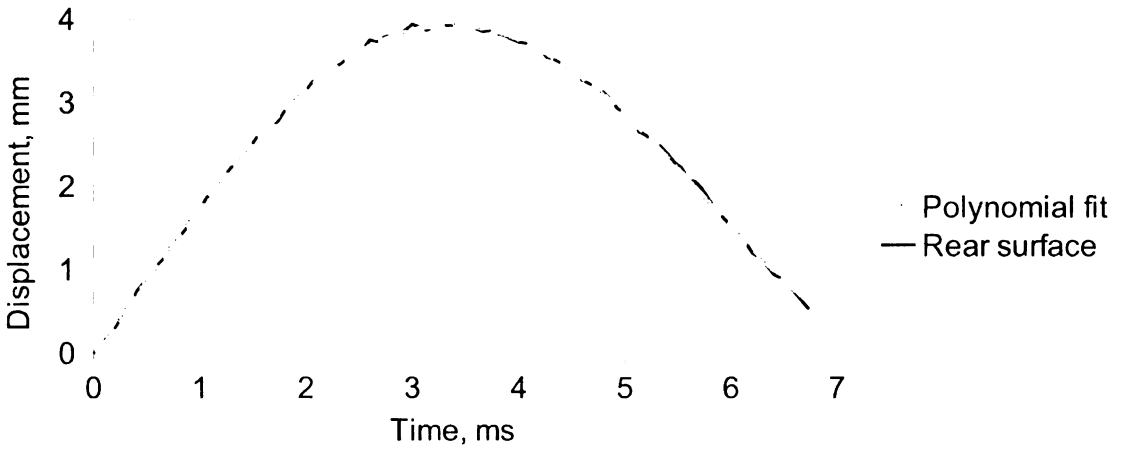

Figure 2.18. Displacement of the rear surface at the impact point and the fitted polynomial.

It is seen in this figure that the displacement trend is captured well by the fifth order polynomial fit. Also, the fitted curve does not contain the noise oscillations present in the original curve. Differentiation of this curve should give good results for velocity and acceleration of the rear surface.

The velocities from the first differentiation of the rear surface displacement and the first integration of the impact surface acceleration are compared in the following figure.

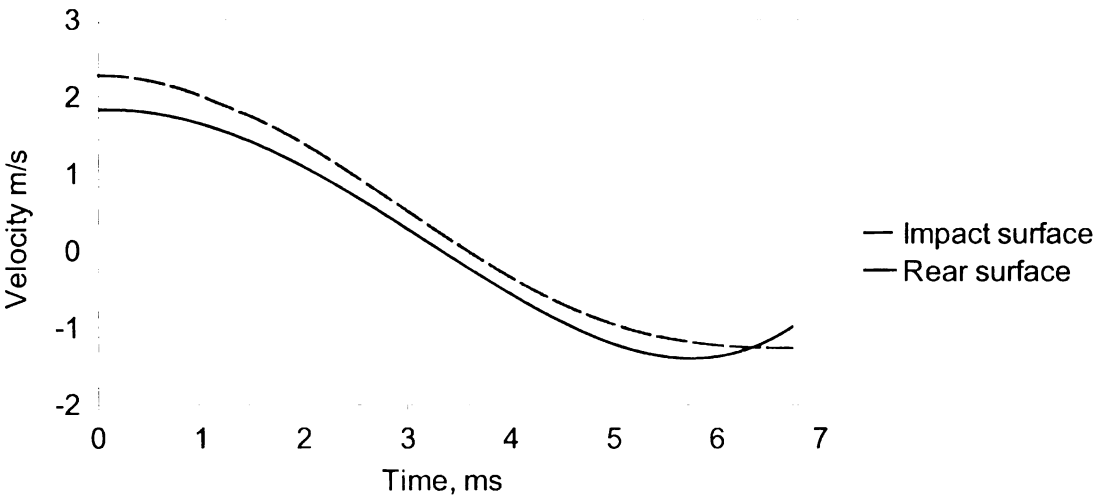

Figure 2.19. Comparison of the velocity of the impact surface and rear surface at the point of impact.

The rear surface acceleration from two time derivatives of the Projection Moiré data and the impact surface acceleration obtained from Newton's Second Law and the assumption of a rigid impacting mass are compared in the following figure.

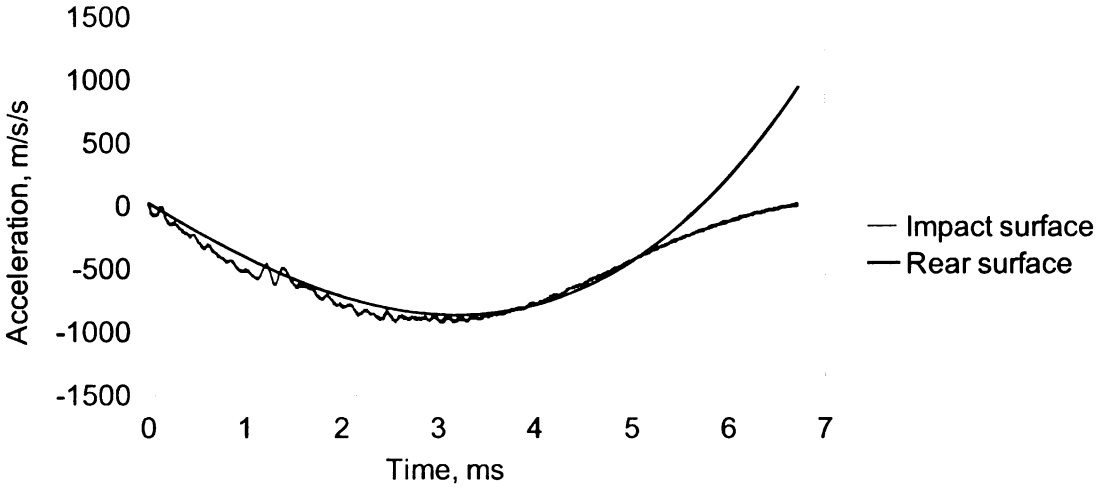

Figure 2.20. Comparison of the acceleration of the impact surface and rear surface at the point of impact.

It is seen in the above figures that both the velocity and acceleration histories of the impact and rear surfaces are reasonably close to each other. It was noted that the impact surface acceleration was never positive. This was due to the fact that this acceleration was obtained from a load cell which could only measure compressive forces.

The results for displacement, velocity, and acceleration for the rear and impact surfaces were all within a reasonable range of each other considering that the two measurements took place on two different surfaces of the specimen. It can be concluded that both techniques give reasonable values for determining each quantity. In order to more fully quantify the reasons for the differences between the quantities, an indentation study on a thinner specimen should be performed with the rear surface unsupported.

2.4 Conclusions

It has been established in this study that Projection Moiré is an acceptable measurement tool for measuring displacement during plate impact testing. The work done by other researchers has streamlined its implementation, and allows for an efficient measurement system.

The full-field displacement provided by the rear surface measurements give a comprehensive evaluation of the specimen. Through observation of these results, it is possible to observe the initiation and growth of major delamination. This was due to the fact that delamination causes a localized degradation of the bending stiffness, and thus a discontinuity in the slope of displacement. The

observations are enhanced by plotting the displacement profile along lines through the impact point. Major delamination is distinguished by a protruded region which forms during the loading portion of the force curve, and grows to its maximum value at the peak force.

The results from the Projection Moiré measurement of the rear surface were compared to the load cell measurements of a single point on the impact surface. The results were quite close to each other considering that the measurements were taken on opposite surfaces in the structure. Since it was known that indentation on the impact surface would cause the results from each surface to be distinct, it was concluded that both techniques give an adequate measurement of the structure's response.

2.5 Future work

The addition of the Projection Moiré setup to the impact of composite plates provides a valuable means for quantifying the rear surface specimen response. Past studies [2.14] have shown the importance of the rear layer in the energy absorbing properties of a composite plate. Future work should use this setup to quantify the performance of different structures by measuring the full-field displacement. Such a study should provide a more thorough understanding of the individual plate's performance and thus a better comparison of alternative materials.

It has been shown in this chapter that the measurements by the load cell on the impact surface and the measurements by Projection Moiré of the rear surface both give reasonable results. Differences between the displacements

has been primarily attributed to the indentation on the impact surface. Indentation tests were conducted on different specimens and a different set of boundary conditions than was used in the impact tests presented in this chapter, however. In order to more fully compare the impact and rear surfaces, indentation tests should be performed using the same specimen as used in this chapter and with the same boundary conditions.

2.6 References

[2.1] Kokidko, D, Gee, L, Chou, SC, and Chiang, FP, "Method for measuring transient out-of-plane deformation during impact," *International Journal of Impact Engineering*, 1996, Vol. 19, 127-133.

[2.2] Chai, H, Knauss, WG, and Babcock, CD. "Observation of damage growth in compressively loaded laminates," *Experimental Mechanics*, 1983, Vol. 23, 329-337.

[2.3] Sutton, MA, McNiell, SR, Helm, JD, and Chao, YJ, "Advances in 2-D and 3-D computer vision for shape and deformation measurements," In: Photomechanics, *Topics in Applied Physics*, Vol. 77, ed. By PK Rastogi, D Inaudi, Elseiver:Oxford, 2000.

[2.4] Reu, PL, VanGoethem, DJ, and Cordova, TE, "Measurement of steel plate perforation tests with digital image correlation," *Proceedings of the SEM Annual Conference,* 2009, Paper no. 144.

[2.5] Tiwari, V, Sutton, MA, Shultis, G, McNeill, SR, Xu, Shaowen, Deng, Xiaomin, Fourney, L, and Bretall, D, "Measuring Full-field Transient Plate Deformation Using High Speed Imaging Systems and 3D DIC," *Proceedings of the SEM Annual Conference* 2009, Paper no. 206.

[2.6] Su, X, Chen, W, "Fourier transform profilometry: a review," 2001, *Optics and Lasers in Engineering*, Vol. 35, 263-284.

[2.7] Zhang, Q, Su, X, Cao, Y, Li, Y, Xiang, L, Chen, W, "Optical 3-D shape and deformation measurement of rotating blaeds using stroboscopic structured illumination," *Optical Engineering,* 2005, Vol. 44, 113601.1-7

[2.8] Su, X, Chen, W, Zhang, Q, Chao, Y, "Dynamic 3-Dd shape measurement method based on FTP," *Optics and Lasers in Engineering,* 2001, Vol 36, 49-64.

[2.10] Paepegem, WV, Shulev, A, Moentjens, A, Harizanova, J, Degrieck, J, and Sainov, V, "Use of projection Moiré for measuring the instantaneous out-of-plane deflections of composite plates subject to bird strike," *Optics and Lasers in Engineering*, 2008, Vol. 46, 527-534.

[2.9] Zhang, Q, Su, X, "High-speed optical measurement for the drumhead vibration," *Optics Express*, 2005, Vol. 13, 3110-3116.

[2.11] Pan, J, and Huang, PS, "Color phase-shifting technique for three dimensional shape measurement," *Optical Engineering*, 2006, Vol. 45, 013602-1 - 013602-9.

[2.12] Chan, PH, Bryanston-Cross, PJ, "Spatial phase stepping method of fringe-patterna analysis," *Optics and Lasers in Engineering*, 1995, Vol. 23, 343-354

[2.13] Heredia, M., and Patterson, E.A., "Location and Shape Measurement Using a Portable Fringe Projection System," *Experimental Mechanics*, 2005, Vol. 45, 197-204.

[2.14] Rosario, K, "Quasi-three-dimensional woven composites," Master's Thesis, Michigan State University, East Lansing, MI, 2008

[2.15] Gulker, B, "Experimental Methods for Impact of Composite Materials," 2009, *Proceedings of the SEM Annual Conference*, Paper no. 575.

Chapter 3: Material properties from impact testing

Abstract

One of the ultimate goals in any material testing is to identify its material properties. If the material is anisotropic, it would require several tests in order to identify each of the material properties. The matter is further complicated when dynamic properties are desired. Since some materials have strain rate dependent material properties, it is desired to establish test methods that will work under dynamic loading. There are methods available which require only one test and will function under dynamic loading. One such method is the Virtual Fields Method. In this study, this method has been applied to plate specimens through the use of numerically simulated data. This simulation allowed for the determination of the best set of boundary conditions for real experiments. Although experimental values for bending stiffness were not found, the general procedure for data processing in experimental implementation is presented. A rigorous study for how to implement this method for real experiments is then proposed.

3.1 Introduction

There are several alternatives available when determining the properties of a material. Traditional tests such as tensile tests can be employed, but require several different testing configurations to fully characterize materials.

The situation becomes more challenging when trying to describe the dynamic material properties if the material of interest is anisotropic. There has

been some work in this field such as with the Split Hopkinson Pressure Bar which can characterize a material, but only with respect to one direction and one strain rate per test. Researchers have also modified drop-weight impact testing equipment for dynamic testing of steel bars [3.1]. Any of these methods would again require the completion of several tests in order to fully characterize the material. There would be additional concerns surrounding the strain rate at which the tests were being conducted. To complete this properly, it would be required that each individual test would have the same strain rate.

In order to move away from the requirement of several individual tests for multiple material properties, researchers have proposed solutions which utilize the full field material response (i.e. displacement, strain, etc.). If the complete material response is known, it is possible to extract many, if not all, material properties from a single test. One such method is the Virtual Fields Method developed by Grédiac and his colleagues [3.2]. In this method, surface strains or displacements are measured as well as the forces acting on the specimen. From these measurements, the material properties can be identified by a series of calculations.

There have been several studies on different test setup conditions using the Virtual Fields Method. Examples of in-plane problems are the most common. For example, static testing has been successful for the following geometries: double notched shear specimen, compression of a thick composite ring, and bending/shear loading of a rectangular specimen [3.2]. In this test, a thick cross section of a filament-wound tube was compressed in one direction. A grid

method was used to measure the displacement on each side of the ring. Since the ring was axis-symmetric, only a section of the ring was measured. The various stiffnesses of the structure were then obtained.

Dynamic in-plane testing has been completed for the tensile loading of a notched composite specimen [3.3]. In this test, a quasi-isotropic composite laminate was tested in a tensile Split Hopkinson Pressure Bar. The Hopkinson Bar was used as a loading mechanism, only. The in-plane displacements were measured using the grid method. Several of the frames of the high speed camera did not have high enough acceleration values, so could not be used in the material property calculation. The results for the Elastic Modulus was about 50% higher than the expected value, and for Poisson's Ratio it was about 10% lower than expected. The low quality of the measurements was deemed to be the reason for the large amount of error. For the Projection Moiré measurements used in the present work, see Chapter 2 for a discussion of the method's accuracy.

There are fewer cases of out-of-plane problems available in the literature, but there are a couple of useful studies available. Grédiac et al. [3.4] studied the bending of a thin anisotropic plate simply supported at 3 of the 4 corners (denoted as SS-3PT in this thesis). In this study, however, the displacement data was not obtained from real test. Rather, the data was simulated using a finite element model. The effect of noisy data was simulated by modifying the curvature values. Two types of noise were simulated. First, the coordinates of the displacement were shifted to simulate an error in setting up a camera. Shifts

of 1% and 5% were considered. Errors in identifying the bending stiffnesses ranged from 0.23 – 10.17% and 1.81 – 129.66%, respectively. Second, uniform random noise was added to the curvature. Random noise of 5% of the maximum curvature was added to each image. Errors in identifying the bending stiffnesses ranged from 0.00 – 31.33 %. It should be noted that if the simulated noise were added to the displacement data instead of the curvature data, it likely that the amount of error would increase. This is because differentiation magnifies the effects of noise.

Grédiac also studied anisotropic plates with free-free boundary conditions under vibration [3.5]. This test, however, required vibration of the specimen at several frequencies to determine all of the bending stiffnesses. In this approach, a plate was excited at its center. The vibration response was simulated using Finite Element Analysis. Steel plates and carbon/epoxy laminates were tested. Each test showed results close to the predicted values. The predicted values were based on static material properties, however. Data was obtained by simulating the experiment in a finite element model. A later study on the same configuration implemented the method for real experiments using deflectometry to measure the slope fields [3.2]. This measurement method provided the advantage of measuring the slopes instead of the displacements. Since the slope data was known, only one differentiation was required to obtain the curvature fields. The specimen was a polycarbonate plate. The extracted elastic modulus showed 4% error from the value obtained from a cantilever beam test. The extracted Poisson's Ratio was not compared to any reference value.

In the initial applications of the method, the virtual fields were selected manually. Some intuition was used in order to obtain fields which were useful. As the method matured, more sophisticated methods were developed. The so-called special virtual fields were defined such that the equations were guaranteed to be independent by uncoupling the equations [3.6]. Since the equations were uncoupled, each bending stiffness could be determined from only one equation. Fields that match this definition are called "special virtual fields." A polynomial expansion is taken to be the general form of the virtual fields. This method, however, requires exploring thousands of possible virtual fields in order to find the ones which provide the highest degree of independence. This increases the computation time.

Avril et al. [3.7] later refined this method by developing the special field which would provide the least sensitivity to noise. It was assumed that the noise in the measurements were random. The requirement that the virtual fields be "special" is maintained, however all of the possible special virtual fields are compared using optimization theory to obtain the ones which posses the least sensitivity to noise.

3.2 Numerical simulation

3.2.1 The Virtual Fields Method

The fundamental theory of the Virtual Fields Method is centered around the Principle of Virtual Work. It will be briefly summarized here. The Principle of Virtual Work is stated as follows [3.2].

$$-\int_V \sigma : \epsilon^* dV + \int_{S_f} T \cdot u^* dS + \int_V f \cdot u^* dV = \int_V \rho \gamma u^* dV \tag{3.1}$$

In this equation, σ is the stress, ε is the strain, T is the traction, u is the displacement, f is the body force, ρ is the density, γ is the acceleration, V is the volume, and S_f is the portion of the surface that the traction is acting on. Any place that has a superscript $*$ indicates a virtual field. According to the principle, this equation is valid for any arbitrary virtual field as long as the virtual field is kinematically admissible (satisfies the boundary conditions).

If it is assumed that the material behavior follows Classical Plate Theory and is orthotropic, the equation can be rewritten as follows.

$$\begin{aligned} &D_{xx}\int_{S_f} k_x k_x^* dS + D_{yy}\int_{S_f} k_y k_y^* dS + D_{xy}\int_{S_f} \left(k_x k_y^* + k_y k_x^*\right) dS \\ &+ D_{ss}\int_{S_f} k_s k_s^* dS + = \int_{S_f} T \cdot u^* dS - \int_V \rho \frac{\partial^2 w}{\partial t^2} u^* dV \end{aligned} \tag{3.2}$$

In this equation, the D's represent the bending stiffnesses, and the k's represent the plate curvatures as described by Classical Plate Theory, e.g. [3.8].

$$k_x = \frac{-\partial^2 w}{\partial x^2};\ k_y = \frac{-\partial^2 w}{\partial y^2};\ k_s = -2\frac{\partial^2 w}{\partial x \partial y} \tag{3.3}$$

If the actual loading, T, and material response is known and the virtual fields, k^*'s and u^*'s, are prescribed, then the only unknowns are the bending stiffnesses. Since there are multiple unknown bending stiffnesses in a given problem, the same number of equations must be generated as the number of unknowns. Different equations can be obtained by applying different virtual fields. This is the fundamental idea behind the Virtual Fields Method.

For the case of an orthotropic plate, four equations have to be generated. Once they are identified, solving for the bending stiffnesses is simply a matrix algebra problem.

$$\begin{bmatrix} \int_S k_x k_x^{*,1} dS & \int_S k_y k_y^{*,1} dS & \int_S \left(k_x k_y^{*,1} + k_y k_x^{*,1}\right) dS & \int_S k_s k_s^{*,1} dS \\ \int_S k_x k_x^{*,2} dS & \int_S k_y k_y^{*,2} dS & \int_S \left(k_x k_y^{*,2} + k_y k_x^{*,2}\right) dS & \int_S k_s k_s^{*,2} dS \\ \int_S k_x k_x^{*,3} dS & \int_S k_y k_y^{*,3} dS & \int_S \left(k_x k_y^{*,3} + k_y k_x^{*,3}\right) dS & \int_S k_s k_s^{*,3} dS \\ \int_S k_x k_x^{*,4} dS & \int_S k_y k_y^{*,4} dS & \int_S \left(k_x k_y^{*,4} + k_y k_x^{*,4}\right) dS & \int_S k_s k_s^{*,4} dS \end{bmatrix}$$

$$\cdot \begin{bmatrix} D_{xx} \\ D_{yy} \\ D_{xy} \\ D_{ss} \end{bmatrix} = \begin{bmatrix} \int_{S_f} T \cdot u^{*,1} dS - \int_V \rho \frac{\partial^2 w}{\partial t^2} u^{*,1} dV \\ \int_{S_f} T \cdot u^{*,2} dS - \int_V \rho \frac{\partial^2 w}{\partial t^2} u^{*,2} dV \\ \int_{S_f} T \cdot u^{*,3} dS - \int_V \rho \frac{\partial^2 w}{\partial t^2} u^{*,3} dV \\ \int_{S_f} T \cdot u^{*,4} dS - \int_V \rho \frac{\partial^2 w}{\partial t^2} u^{*,4} dV \end{bmatrix} \tag{3.4}$$

This equation can be expressed symbolically as follows.

$$AD = B \tag{3.5a}$$

$$D = A^{-1} B \tag{3.5b}$$

If the matrix A is independent, then the vector D should be comprised of the plate bending stiffnesses.

Prior to implementing this method for real experiments, it was desired that the method be explored using numerically simulated data. This was done for two primary reasons. First, it confirmed that the method was valid for the desired loading configuration. Second, it provided a tool for comparing alternative

boundary conditions. This allowed for the determination of the best experimental setup available.

3.2.2 Numerical study using simulated data

It has been seen in the literature [3.4] that the SS-3PT boundary condition (as defined in Figure 3.1) provides good results for obtaining the bending stiffnesses. This, however, is not a realistic boundary condition for impact testing. Since the ultimate goal of this study is to apply the Virtual Fields Method to plate impact testing, an effective set of boundary conditions must be identified. Traditionally, the boundary conditions which have been used in drop weight testing is such that all four edges of a plate specimen are clamped. This is much more repeatable than trying to implement some sort of simply supported condition.

In this study, several boundary conditions were studied as well as two different methods for defining the virtual fields. The following flowchart outlines the procedure for evaluating each case.

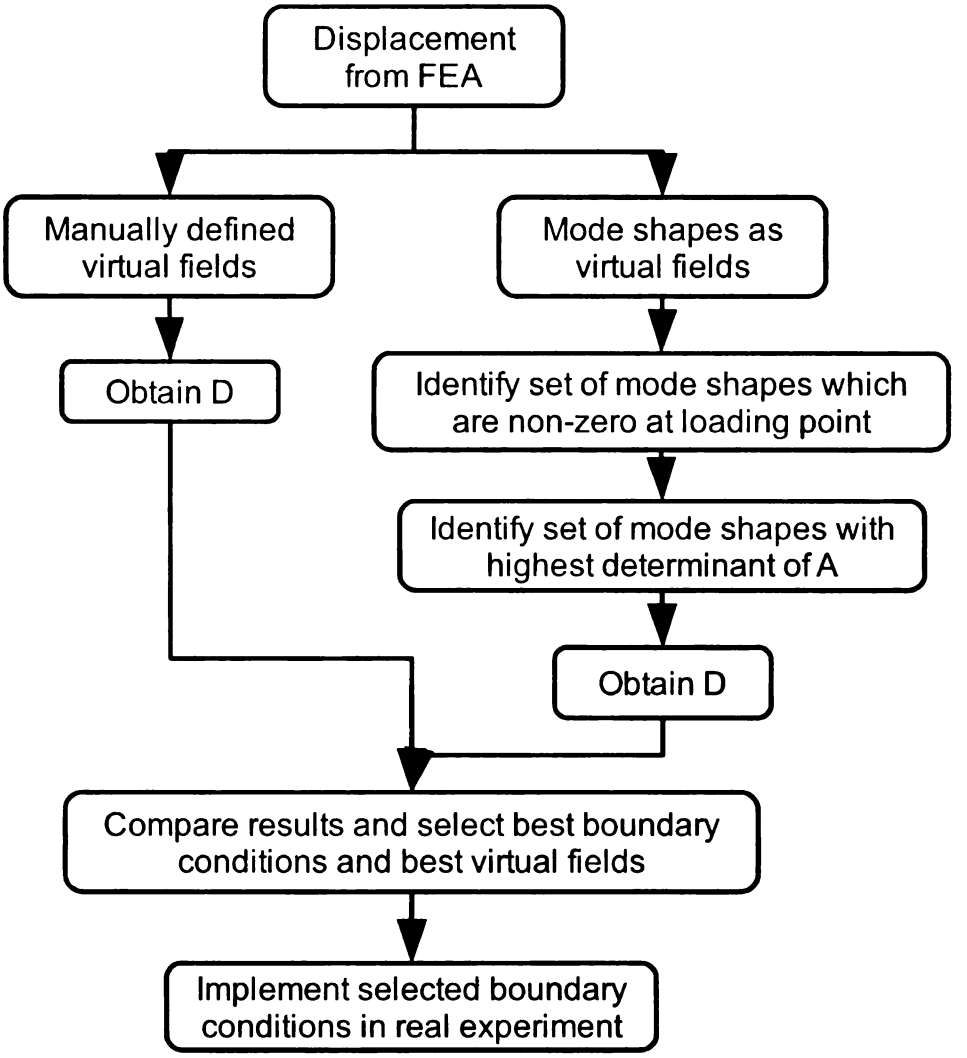

Figure 3.1. Flowchart outlining the study conducted using the Virtual Fields Method.

The displacements obtained from FEA were for static loading. Although the displacement in impact testing would be different in some ways, the overall trends in the displacement should be similar for the elastic portion of the impact event. For this reason, it was assumed that the set of boundary conditions identified from the static, numerical study could be extended to impact testing.

3.2.2.1 Alternative boundary conditions

Since it is feasible for real experiments, the clamped boundary condition was explored to understand its usefulness. For completeness, simply supported boundary conditions were also explored as well as various combinations of supported edges. The image below outlines the various boundary conditions explored in this study as well as introduces the notation used to describe them. In this image, the solid triangles (▲) represent a simply supported boundary condition and the hash marks ( ) represent a clamped boundary condition.

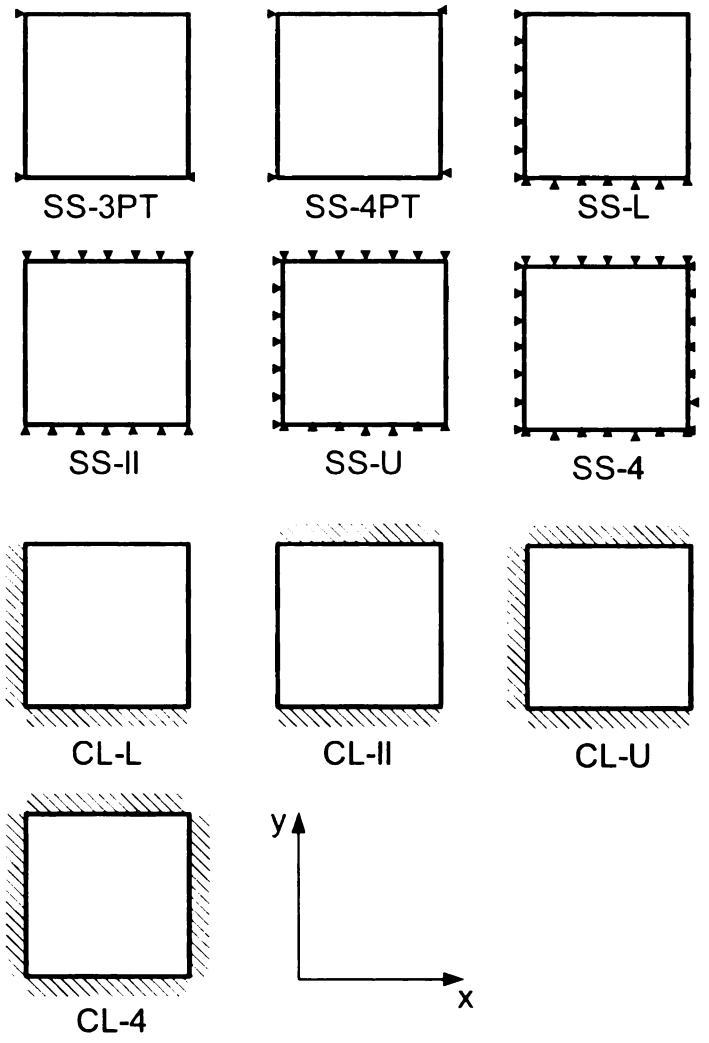

Figure 3.2. Schematics and notation definition of alternative boundary conditions explored in the numerical portion of the study.

A numerical study was performed to to demonstrate the method and identify an effective experimental setup. Sor simplicity, a static finite element model was built using Abaqus CAE in order to determine the static bending response of each case. Once the best setup was determined by the numerical study, that set of boundary conditions could be applied to real tests with confidence. The finite element mesh used in this study was composed of 100x100 square shell elements (S4R in Abaqus). The material was defined as a

single orthotropic layer with material properties of E_{11} = 40 GPa, E_{22} = 10 GPa, G_{12} = 4 GPa, and ν_{12} = 0.3. Since the material properties had to be an input to Abaqus, the exact bending stiffnesses could be calculated using Classical Laminate Theory [3.8]. Since the model was for a single layer, the bending stiffnesses can be calculated as follows.

$$D_{ij} = \frac{1}{3} Q_{ij}^{L} \left(z_{L}^{3} - z_{L-1}^{3} \right) \tag{3.7}$$

In the formula above, *z* is the through thickness direction with zero defined at the middle of the plate (with respect to its thickness), *L* is the layer number, *n* is the number of layers (in this example *n*=1), and *Q* is defined as follows.

$$S = \begin{bmatrix} \frac{1}{E_{11}} & \frac{-\nu_{12}}{E_{11}} & 0 \\ \frac{-\nu_{12}}{E_{11}} & \frac{1}{E_{22}} & 0 \\ 0 & 0 & \frac{1}{G_{12}} \end{bmatrix} \tag{3.8}$$

$$Q = S^{-1} \tag{3.9}$$

In the above equations, *1* and *2* are defined as the fiber and matrix directions of the laminae, respectively. *E*, *G*, and *ν* are Young's Modulus, shear modulus, and Poisson's Ratio of the laminae, respectively. The bending stiffnesses resulting from the prescribed material properties were as follows.

$$D_{xx} = 0.85 \ N \cdot m$$
$$D_{yy} = 3.41 \ N \cdot m$$
$$D_{xy} = 0.26 \ N \cdot m$$
$$D_{ss} = 0.33 \ N \cdot m$$

The results from the Virtual Fields Method could then be compared to these reference values.

3.2.2.2 Virtual field selection

In order to solve the system of equations developed by applying different virtual fields, it is necessary that the equations be independent. The independence of these equations is related to the independence of the defined virtual fields. As a first step , the virtual fields were defined manually. It is difficult, however, to successfully define these fields manually while obtaining independence. For this reason, it is desired that an objective means of defining independent virtual fields is desired. In order to refine the field selection, the free vibration mode shapes were selected as the virtual fields. These mode shapes were obtained using the same finite element model as used for the displacement calculation. Several mode shapes were obtained and various combinations of four of them were explored. In most of the cases explored here, the first six mode shapes were obtained. The results for each set of boundary conditions and for each field selection technique were compared in order to determine the best configuration for the real experiments.

3.3 Experimental implementation

An outline of the general procedure which should be followed in implementing the Virtual Fields Method for plate impact testing is outlined below. Tests were run, and calculations made on the obtained data. However, first attempts at extracting the material properties from this test were unsuccessful, as will be discussed in the subsequent sections. The likely reasons for the errors are discussed in the Results and Discussion section. Additionally, a thorough proposal for future study is presented. Future work should use the methods and results used in this chapter as a starting point to refine the procedure.

3.3.1 Drop-weight impact testing

Impact testing was carried out on the drop-weight impact tester (DWIT). Projection Moiré measurements were used to obtain the full field out-of-plane displacement data. Details of the setup and procedure can be found in Chapter 2 of this thesis. Since the goal is to find the elastic material properties, care must be taken to ensure that the time step used to obtain the bending stiffnesses is such that damage has not initiated. The results of Chapter 2 concerning the protruded region should be taken into consideration in the present study.

3.3.2 Data processing

Implementing the method for real test data, as opposed to simulated data, introduces additional complications. In the experiment, the full field out-of-plane displacement is obtained. It is the curvature data, however, that is desired.

Since the plate is thin, as long as the deformation is elastic, Classical Plate Theory can be used to calculate the plate curvatures as outlined in Equation (3.3).

3.3.2.1 Filling in unknown region

Due to the configuration of the fixture and the angle of the light projection, there was a portion of the specimen which was not illuminated during the test. This was due to the position of Mirror 2, as shown in the following schematic.

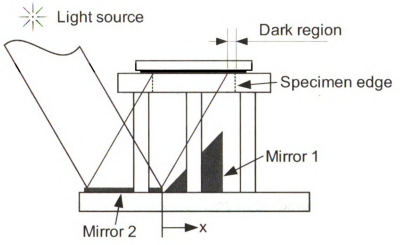

Figure 3.3. Schematic of how the restrictions on the mirror positioning limited the portion of the specimen which could be viewed.

In order to be able to illuminate the entire specimen while still maintaining the desired projection angle, Mirror 2 should be shifted in the positive x direction. However, the dimensions of Mirror 1 did not allow for this. Future work should include refining the mirror dimensions and positions.

The following displacement plot from the experiment shows the result of this in the experimental data (Regions A and B).

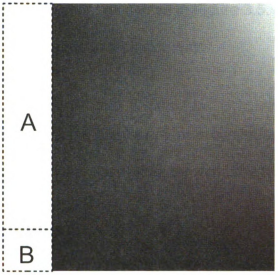

Figure 3.4. Regions A and B indicate portions of the specimen which could not be viewed due to shadows produced by the light projection angle.

Future testing should involve refinement of the testing fixture to allow for the complete specimen to be viewed. This could be done by optimizing the mirror dimensions and locations. For the present study, however, these regions were filled according to an assumed displacement field. Since the displacement in Regions A and B is known to be near zero due to the clamped boundary condition, this should not effect the results significantly. Since the Virtual Fields Method requires the full-field response, we assume displacements in these regions to be

$$w_i = a_i x^2 \tag{3.10}$$

in region A where i indicates the row number and a is such that the displacement is continuous between the known and unknown regions. This function was chosen due to its consistency with the slope of the actual displacement in the

measured portion of the specimen, as shown in Figure 3.5. For region B, the displacement pattern is assumed in a similar way.

$$w_i = b_i x^2 y^2 \tag{3.11}$$

In this equation, b is such that the displacement is continuous across each region. It was also observed that the slopes between the two regions is consistent (Figure 3.5).

Profiles for several time steps were drawn through region A at the impact point to show how the assumed shape of the unknown region compares with the portion of the specimen which was visible. These profiles are shown in the following image for several early time steps.

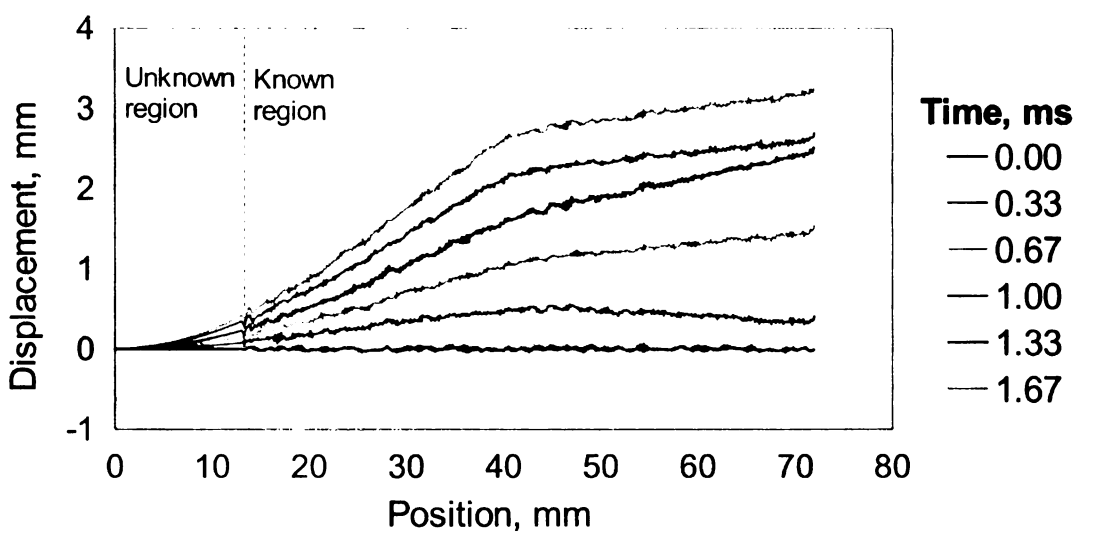

Figure 3.5. Displacement profiles through the impact point for the raw data and filled regions.

Although the method of filling the unknown regions is not ideal, it allows for the use of the current test setup without modification. It is acceptable for this testing since the displacements in the unknown region are near zero due to their proximity to the boundary. Future testing and refinement of the experimental

procedure should include refinement of the test setup to eliminate this issue from the analysis.

3.3.2.2 Spacial smoothing

Since differentiation is sensitive to noise, the displacement data must be smoothed in order to ensure that the curvature calculations are useful. There are a variety of methods available for data smoothing, each suited to specific situations. In this study, there are no sudden changes in slope of the data as long as the deformation under investigation is prior to the damage initiation. For this reason, a simple central moving average approach is used. In this method, the value at each pixel (point of data in an image) is smoothed by taking the average of the pixels in the region around that pixel. This calculation is performed for each pixel with respect to the original image. The size of the region is defined by the user. Smaller regions are more true to the original image, but less smooth. Several region sizes were explored. It was found that a square region with sides lengths of 30 pixels (15 pixels in each direction) was the best for this study since it smoothed the data adequately for differentiation as well as matched the original data. Since there are many frames of data to be analyzed when the high speed camera is used, the computational efficiency of this method is beneficial. A comparison between the raw and smoothed data is shown below for a typical time step.

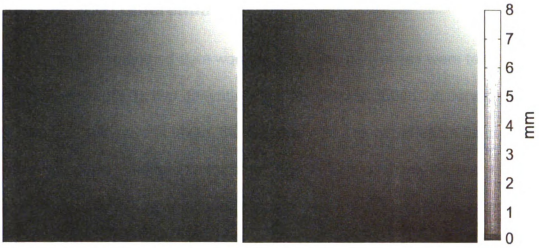

Figure 3.6. Comparison between unsmoothed (left) displacement from Projection Moiré and the smoothed results (right) from the central moving average.

In order to ensure that all of the relevant features of the data are captured, a profile through the impact point is drawn for each frame of displacement up to delamination initiation. The impact point is chosen because it is the point where the slope is the steepest. It is assumed here that delamination is the first damage mode to have a significant effect on the material properties of the plate.

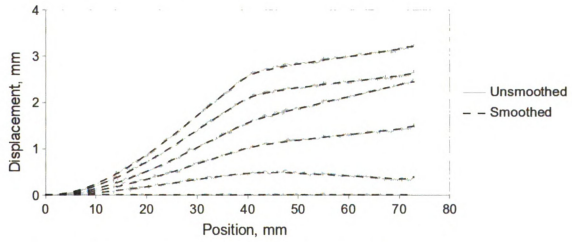

Figure 3.7. Displacement profile through the impact point comparing the unsmoothed and smoothed data for different times. The time step between lines is 0.33 ms.

3.3.2.3 Spacial differentiation

Once the smoothed data was obtained, the derivatives were taken. As seen in Equation (3.3), two derivatives are required to obtain the curvatures. After the first derivative is taken, the data must be smoothed again before the second derivative is taken. In this study, the same smoothing method was used at each step. Curvature results for a typical time (t = 1.33 ms) step are shown below.

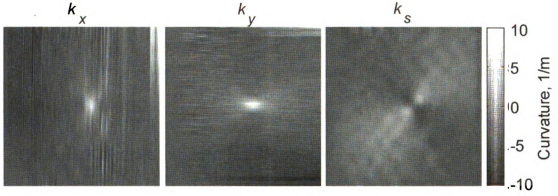

Figure 3.8. Curvature fields for a typical time step for the CL-L boundary conditions

It is seen that the results for k_x and k_y both vary in a similar way between the clamped and free edges. The results for k_s show results which are nearly symmetric with respect to the diagonal which is what was expected. Profile lines through the impact point along the diagonal for each curvature field are shown in the following figures.

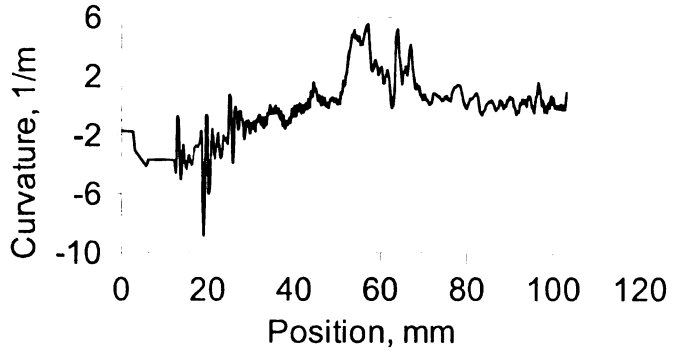

Figure 3.9. Profile through the impact point for k_x

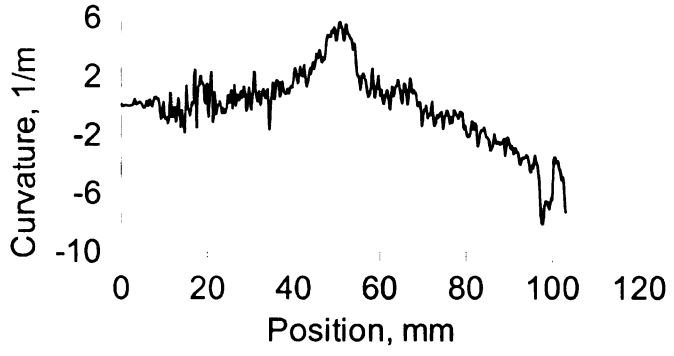

Figure 3.10. Profile through the impact point for k_y

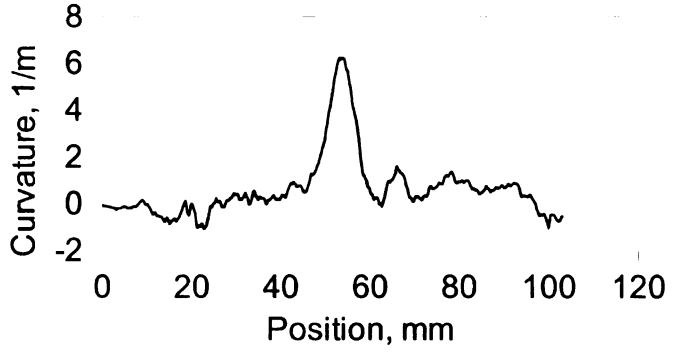

Figure 3.11. Profile through the impact point for k_s

The figures above show the high degree of noise which is present in the curvature results. The plot for k_s showed less noise due to the fact that calculating k_s involves differentiation in two directions. This has somewhat of a

smoothing effect. If two derivatives are taken in the same direction, the amount of noise present in the results is much greater, as seen in the plots for k_x and k_y. Due to the noise, it is difficult to identify exactly what the trend is in each of the curvature results.

3.3.2.4 Temporal smoothing and differentiation

In addition to differentiation required for the calculation of curvatures, it is also necessary to perform differentiation with respect to time in order to calculate the accelerations. In order to do this, it is necessary for the data to be smooth with respect to time. The methods for smoothing and differentiating this data were presented in Chapter 2 of this thesis. In the previous discussion, only the point of impact was considered. For the current discussion, however, the full field acceleration is required. In order to obtain this, the procedure discussed in Chapter 2 was implemented for every data point (every pixel of the set of images). The following figure shows an acceleration field for the CL-L (two adjacent edges clamped) test configuration at a typical time step using the described approach.

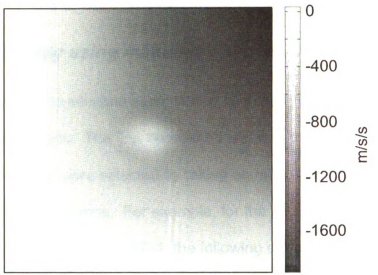

Figure 3.12. Example of acceleration fields for the CL-L plate.

3.3.2.5 Virtual field selection

The method of applying the mode shapes as the virtual fields was investigated for use in experimental implementation. One difference here, however, is that the specimen material properties are not known prior to testing. Therefore, the exact material properties cannot be input to Abaqus in determining the mode shapes. This is not a problem, however, since the virtual fields may be arbitrary. Therefore, the results should be independent of the material properties used in determining the mode shapes. In order to maintain consistency, generic material properties for glass/epoxy laminates were input to the Abaqus model. This ensures that the mode shapes obtained are for an orthotropic material.

3.4 Results and discussion

3.4.1 Numerical study using manually defined virtual fields

Abaqus was used to simulate static testing of thin orthotropic plates with various boundary conditions. The first approach used was to manually define the virtual fields. These fields were selected by taking equations which were known to satisfy the boundary conditions. For example, for the case of a plate simply supported at each of its for corners, SS-4, the following equations were used.

$$\begin{aligned} w^{*,1} &= x^3(x-L)^3 y^3(y-L)^3 \\ w^{*,2} &= \sin\left(\frac{\pi}{L}x\right)\sin\left(\frac{\pi}{L}y\right) \\ w^{*,3} &= \left(e^{xy}-1\right)\left(e^{(x-L)(y-L)}-1\right) \\ w^{*,4} &= x^5(x-L)^5 \sin\left(\frac{\pi}{L}y\right) \end{aligned} \tag{3.6}$$

For different boundary conditions, the equations were modified so as to match the boundary conditions for a given problem. Although these equations may not guarantee independence of the matrix to be inverted, they serve as a starting point for utilizing the Virtual Fields Method. The results are shown in the table below.

Table 3.1. Bending stiffness results when virtual fields were manually defined.

	D_{xx}	D_{yy}	D_{xy}	D_{ss}	err_{xx}	err_{yy}	err_{xy}	err_{ss}
Reference	0.85	3.41	0.26	0.33	-	-	-	-
SS-3PT	0.86	3.11	0.33	0.33	0.30	-8.69	27.56	-1.20
SS-4PT	0.87	3.43	0.26	0.30	2.42	0.46	1.45	-9.51
SS-L	0.91	3.54	0.25	0.25	6.84	3.66	-2.54	-25.98
SS-II	0.97	3.37	0.56	0.12	13.75	-1.07	120	-63.97
SS-U	-0.22	3.75	1.05	0.30	-126	10.03	311	-10.71
SS-4	0.87	3.44	1.06	-0.05	1.87	0.88	315	-115
CL-L	2.47	6.05	15.05	2.67	189	77.50	5784	700
CL-II	2.27	4.67	-283	141	166	36.98	-110899	42092
CL-U	2.03	4.54	-338	168	139	33.12	-132208	50308
CL-4	2.68	5.81	2394	-1199	214	70.39	935795	-359927

Since the finite element model was for laminated composite materials, the Reference values were determined using Equations (3.7-9).

There are a few observations to be made based on this table. First, it is seen that the results for the clamped boundary conditions are fail, whereas a large portion of the simply supported boundary conditions provide favorable results. This is likely due to the difficulty in defining the virtual fields manually as the boundary conditions become more restrictive. This is reasonable since it is known that for in-plane testing, the contribution of the different stress components will influence the identifiability of the different material properties [3.2].

An additional observation is made when comparing the bending stiffness results to the degree of symmetry present in the boundary conditions. The simply supported cases are explored here since they are the only ones which gave favorable results. The boundary conditions are shown below with lines drawn for the various lines of symmetry.

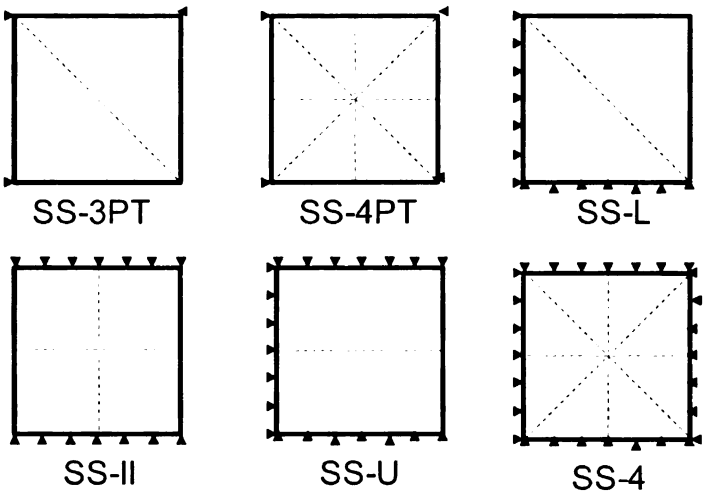

Figure 3.13. Comparison of the degree of symmetry present in each of the simply supported boundary conditions. The dotted lines represent lines of symmetry.

The single exception to this observation is the SS-4PT boundary condition. This can be explained, however, by the lesser degree of restrictiveness of this case when compared to the cases of support along an entire edge.

3.4.2 Numerical study using mode shapes as virtual fields

In order to define a more robust method for defining the virtual fields, the mode shapes of each boundary condition were used as the virtual fields. Since several mode shapes were determined, there were a variety of combinations that are possible for the selection of four virtual fields. As a starting point, the first six mode shapes were explored as possible virtual fields.

It was determined that the best results were obtained when the displacement of the virtual field was non-zero at the location of loading. If the displacement is zero, then the right hand side of the equation goes to zero. The resulting bending stiffnesses in this case are not meaningful. There was one

observed exception to this trend (the CL-U case) which will be discussed later in this section.

As an example of the method, the mode shapes for the CL-L condition are shown below. For each mode shape, it was observed that the displacement at the center of the plate was non-zero. Therefore, any combination of them should work, provided that matrix A is independent. In order to rank the various possible combinations of mode shapes, matrix A was assembled and the determinant was calculated. The combination which provided the highest determinant of matrix A was taken to solve for the bending stiffnesses. The combination with the highest determinant for matrix A was chosen since a high determinant suggests that the equations which make up matrix A are independent.

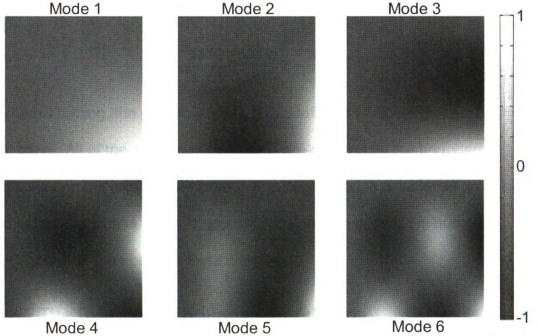

Figure 3.14. The first six mode shapes for the CL-L case. The specimen orientation is the same as Figure 3.6.

The same procedure was followed for each of the remaining boundary conditions. The results are summarized in the table below.

Table 3.2. Results for numerical study of alternative boundary conditions based on static loading using simulated data. Four mode shapes ere selected as virtual fields. Definitions of boundary conditions can be found in Figure 3.1.

	D_{xx}	D_{yy}	D_{xy}	D_{ss}	err_{xx}	err_{yy}	err_{xy}	err_{ss}
Reference	0.85	3.41	0.26	0.33	-	-	-	-
SS-3PT	0.86	3.67	0	0.33	0.46	7.76	-101	-1.32
SS-4PT	2.21	39.76	-0.2	-8.23	159	1066	-178	-2568
SS-L	0.85	3.43	0.27	0.33	0.23	0.45	6.23	-0.4
SS-II	2.25	6.64	-11.92	8.43	163	94.68	-4759	2428
SS-U	0.89	3.45	0.29	0.31	4.14	1.27	13.87	-5.85
SS-4	0.2	-1.74	7.3	-1.65	-76.16	-151	2754	-595
CL-L	0.91	3.73	0.23	0.3	6.3	9.38	-8.29	-10.83
CL-II	2.38	1.75	10.69	-3.56	179	-48.61	4081	-1168
CL-U	1.07	4.02	-1.7	0.94	25.87	17.94	-766	182
CL-4	2.25	4.56	-12642	6319	164	33.59	-4942257	1895910

In dynamic testing, the general shape of the deflection is the same as for the static case. All of the symmetry conditions are dictated by the boundary conditions and the location of loading. For this reason, it is believed that the set of boundary conditions which is determined to be the best in the numerical simulation is also the best for impact testing.

3.4.2.1 The CL-U set of boundary conditions

It was stated in the previous section that the CL-U case proved an exception to the trend that the virtual field should be non-zero at the location of loading. When the mode shapes with non-zero values at the load location were

selected (modes 1, 2, 3, and 6), the results were unfavorable. This is seen in row 2 of Table 3.3. However, when modes 1, 2, 4, and 5 were used, row 3 of Table 3.3, the bending stiffness results were quite good. Note that modes 4 and 5 have zero values at the loading point. The first six mode shapes are plotted below.

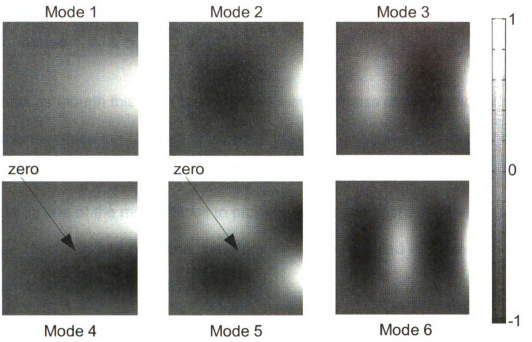

Figure 3.15. The first six mode shapes for the CL-U case. The specimen orientation is the same as Figure 3.6.

The results for the highest determinant case, the non-zero case, and the "best" results are shown below. The "best" results were determined by examining all combinations of the six mode shapes and identifying the option which possessed the smallest total error, row 4 of Table 3.3. It is seen that all cases possess a high degree of error, but the expectation was that the smallest error should be when the mode shapes with the non-zero values at the load point were used. This, however, was not the case.

Table 3.3. Comparison of results for the CL-U case using different combinations of mode shapes

		D_{xx}	D_{yy}	D_{xy}	D_{ss}	err_{xx}	err_{yy}	err_{xy}	err_{ss}
1	**Reference**	0.85	3.41	0.26	0.33	-	-	-	-
2	**Non-zero at load; Modes 1, 2, 3, 6**	1.07	4.02	-1.70	0.94	25.87	17.94	-766	182
3	**Highest det; Modes 1, 3, 5, 6**	0.68	3.33	2.16	-0.33	-20.51	-2.27	742	-199
4	**"Best" results; Modes 1, 2, 4, 5**	0.52	3.69	0.51	0.39	-39.16	8.18	97.46	17.76

It seems as though this must be due to the restrictiveness of the boundary conditions. Since the CL-U case is one of the most restrictive, based on the number of restricted edges and type of boundary conditions, it follows that it should be one of the most difficult to properly identify an appropriate set of virtual fields. This boundary condition, therefore, should be avoided in the experimental implementation of the method.

3.4.2.2 The CL-4 set of boundary conditions

The most frequently used configuration for impact testing in past studies has been one in which each edge of the specimen is clamped. This was due to the fact that clamped boundary conditions are easiest to obtain in real experiments. Additionally, the symmetry of the problem made it relatively easy to analyze compared with alternative boundary conditions. It is found in this study, however, that the CL-4 set of boundary conditions produces unfavorable results when implementing the VFM.

It has been demonstrated in the previous sections that increasing the restrictiveness (based on number and type of boundary conditions) of the boundaries reduced the accuracy with which the bending stiffnesses could be identified. Also, increasing the amount of symmetry in the specimen decreased the quality of the results. Since the CL-4 is both the most restrictive (four clamped edges) and has the highest degree of symmetry, it does not give favorable results for the bending stiffnesses. Although CL-4 has been used extensively in past studies, it is not a good candidate for the determination of plate bending stiffnesses.

3.4.2.3 Refinement for the CL-L set of boundary conditions

From the above study, it is concluded that the most appropriate set of boundary conditions for further study is the CL-L condition. From past experience, it is known that clamped boundary conditions are the only practical choice for real experiments, and the L configuration has proven to be the most favorable for the implementation of the Virtual Fields Method.

Since the CL-L boundary condition has been selected as the setup of choice for future use, it was desired to determine how this technique could be enhanced by considering additional mode shapes. The number of mode shapes considered was expanded to the first twenty. Again, the combination of four mode shapes which provided the highest determinant of matrix A was taken as the best solution. It was found that the highest determinant was found when mode shapes 3, 4, 10, and 11 were used as the virtual fields. The table below compares the results.

Table 3.4. Comparison of the results obtained for the CL-L case when the first six modes are considered and when the first twenty modes are considered.

	D_{xx}	D_{yy}	D_{xy}	D_{ss}	err_{xx}	err_{yy}	err_{xy}	err_{ss}
Reference	0.85	3.41	0.26	0.33	-	-	-	-
Using modes 1-6	0.89	3.51	0.68	0.42	4.64	2.82	164	26.83
Using modes 1-20	0.90	3.73	0.23	0.30	6.15	9.45	-9.07	-10.77

3.4.3 Experimental implementation

3.4.4 Sources of error

The results of the experiments study did not provide useful values for the bending stiffnesses. As different combinations of mode shapes were selected as the virtual fields, there was significant scatter in bending stiffness results. For this reason, it was concluded that substantial work was still needed.

Among the sources of error was the amount of noise present in the curvature plots. This can be seen by observing Figures 3.8-11. In this set of images, there is a great deal of oscillation in the resulting values. The noise present in the curvature results is more severe than was present in the displacement data from which it was calculated. This is due to the fact that differentiation magnifies the effects of noise. Future work should focus both on further reducing the amount of noise in the original image as well as on better smoothing techniques. It should be noted that the noise did not negatively effect the acceleration calculation as much as the curvature calculation. This can be seen by examining the comparison of the impact and rear surfaces in Chapter 2

of this thesis. Apparently, the smoothing technique used for the acceleration calculation was more effective.

An additional source of error in this test is the section of the specimen which could not be viewed by the high speed camera as shown in Figure 3.3. In order to properly implement the proposed method, the fixture should be refined by optimizing the position and size of the mirrors such that the entire specimen is illuminated.

3.5 Conclusions

The method of using mode shapes as virtual fields was found to perform better than the method of manually selecting functions to use as virtual fields. In part, this was due to the fact that, by selecting mode shapes as the virtual fields, it is guaranteed that the fields were independent. Additionally, it provided a more objective method for virtual field selection than semi-arbitrarily manual fields. In the numerical study of alternative boundary conditions, it was found that the method of selecting mode shapes provided results which were consistently more accurate than the method of manually defining the virtual fields. Finally, the mode shapes method allowed for the identification of bending stiffnesses in the case of clamped boundary conditions, whereas the method of selecting the virtual fields manually failed for each of the clamped cases. Since clamped cases are more practical to implement in real experiments than simply supported, the method of selecting mode shapes as virtual fields is the better choice.

It was found that the CL-L set of boundary conditions provided the best results for applying the Virtual Fields Method for the current loading scenario.

The selection of this case was a result of finding a balance between the following contributing factors.

1. The best results are obtained when the boundary conditions are less restrictive. For example, better results are obtained with simply supported than with clamped boundary conditions.
2. The selected set of boundary conditions must be selected such that each bending stiffness influences the plate response significantly enough. For example, The CL-L configuration performs better than the CL-4 configuration since CL-4 is not sensitive to twisting.
3. The selected set of boundary conditions must be practical for experimental implementation. For example, clamped edges can be implemented simply and consistently in experiments whereas simply supported edges cannot.

Although the numerical study was based on static loading, it is thought that the configuration should also be the best configuration for dynamic loading. This conclusion is due to the fact

3.6 Future work

The methodology presented in this chapter for implementing the Virtual Fields Method needs further refinement. It was seen that the curvature fields contained a large amount of noise. Further study needs to be conducted to reduce this. Future work should focus on reducing the noise in the displacement data as well as on alternative techniques to smooth the data before differentiation. In addition to the data processing, the fixture design needs to be refined. Presently, the entire specimen is not illuminated by the grating

projection system. The fixture needs to be refined in order to obtain the optimum size and location of the mirrors for the prescribed projection angle.

In order to apply the Virtual Fields Method to impact testing, it is proposed that several intermediate studies be carried out. First, experiment should be run for static loading cases. This should validate the findings of the numerical approach used in this thesis study. Upon completion of the static case, quasi-static simulation and testing should be conducted. This should then be followed by impact simulation and testing. Each of the simulations should resemble the numerical method used in this thesis.

By conducting this incremental study, the problem would become more complex at each step. For example, the static testing results would not include acceleration calculations. Potential sources of error may be identified and corrected in each stage of the study. Therefore, the procedure could be refined step-by-step before finally implementing the impact test.

In addition to being a useful study for refining the method, it would provide valuable insight into the influence of strain-rate on the materials. If the same specimen was used for each of the three loading cases, then the material properties extracted at each stage should provide a portrait of the material's performance under different loading rates.

3.7 References

[3.1] Shin, H.-S., Lee, H.-M., and Kim, M.-S., "Impact tensile behaviors of 9% nickel steel at low temperature," *International Journal of Impact Engineering*, 2000, Vol. 24, 571-581.

[3.2] Grediac, M, Pierron, F, Avril, S, and Toussaint, E, "The Virtual Fields Method for Extracting Constitutive Parameters From Full-Field Measurements: A Review," *Strain*, 2006, Vol. 42, 233-253.

[3.3] Moulart, R, Pierron, F, Hallett, SR, and Winsom, MR, "Full-field strain measurements at high rate on notched composites tested with a tensile Hopkinson bar," 2009, *Proceedings of the SEM Annual Conference*, Paper no. 176.

[3.4] Grediac, M, Toussaint, E, and Pierron, F, "Special virtual fields for the direct determination f material parameters with the virtual fields method. 3. – Application to the bending rigidities of anisotropic plates," *International Journal of Solids and Structures*, 2003, Vol. 40, 2401-2419

[3.5] Grediac, M, and Paris, PA, "Direct Identification of Elastic Constants of Anisotropic Plates By Modal Analysis: Thoeretical and Numerical Aspects," *Journal of Sound and Vibration*, 1996, Vol. 195, 401-415.

[3.6] Grediac, M, Toussaint, E, and Pierron, F, "Special virtual fields for the direct determination f material parameters with the virtual fields method. 1. – Principle and definition," *International Journal of Solids and Structures*, 2002, Vol. 39, 2691-2705.

[3.7] Avril, S, Grédiac, M, and Pierron, "Sensitivity of the virtual fields method to noisy data," *Computational Mechanics*, 2004, Vol. 34, 439-452.

[3.8] Daniel, I, and Ishai, O. Engineering Mechanics of Composite Materials. New York: Oxford University Press, 2006.

Chapter 4: Translucent composites for studying damage progression

Abstract

Translucent glass/epoxy specimens can be made by using fiber and matrix with a similar index of refraction. This technique was used to make specimens for impact testing. Since the specimen was transparent enough, it was possible to see the delamination growth within the specimen during the impact event by using a high speed camera. This information could then be compared to the force history. Since delamination can be observed as a function of time, it was possible to estimate the crack speed between images. Additionally, methods for implementing the Projection Moiré method at the same time as observing the delamination were explored. Partially painted specimens and semi-transparent paint were used. It was found that both measurements can be implemented at the same time effectively, but it is difficult to obtain the correct balance between transparency and opacity. This problem may be easier to solve over time as high speed camera light sensitivity continues to improve.

4.1 Introduction

In addition to the deflection and force measurements which have been established in the previous chapters, it would be greatly beneficial to measure the damage progression within the composite material during the impact event. Takeda et al [4.1] conducted a study in which light was transmitted through the specimen during ballistic loading. The light allowed for the observation of the

total delaminated region which was recorded by a high speed camera. Since the specimen was not transparent, however, the study was limited. As the specimen thickness increases, the amount of light which can be passed through the specimen decreases, and the visibility of the delamination diminishes.

This would be greatly enhanced if the degree of transparency was increased. It is possible to make glass/epoxy composites which are very close to transparent if the index of refraction of the fiber and matrix is very close, if not identical. Details about how this can be achieved in VARTM manufacturing of composite materials can be found in the work by Dhyani [4.2].

In addition to observing the damage evolution within the composite, it would be beneficial to perform Projection Moiré measurements simultaneously in order to more fully quantify the material's behavior. In order to obtain this, it is necessary to find a balance between complete transparency which is good for observing internal damage and complete opaqueness which is good for Projection Moiré measurements.

4.2 Methods

The method for impacting these specimens was the same as outlined in Section 2.2 of this thesis. The specimens were made with sufficient transparency by the same procedure as used by Dhyani [4.2]. Two types of specimens were tested – woven composites and cross-ply laminated composites. The woven composites were manufactured by stacking several 0/90 plain-weave layers together. The laminated composites were manufactured by

aligning yarns to make individual single-direction layers. These layers were then stacked together to create a cross-ply laminate.

The optimal setup for observing the internal damage is a completely transparent specimen. In contrast, the optimal setup for Projection Moiré measurements is a fully opaque in order to reflect the maximum amount of light possible. In order to reach a compromise, two techniques were used. One approach utilized the symmetry of the material and the boundary conditions. Half of the specimen was coated in matte white paint and the other half was left unmodified. In the other approach, a semi-transparent white paint (Plaid Pearlcote) was used to coat the rear surface. Since the coating was only semi-transparent instead of matte white, not as much light was reflected from the surface. This reduced the maximum frame rate which could be used by the high speed camera while still recording an image. Additionally, the semi-transparent paint used in this study had a glossy finish. This produced undesired glare in the images. In order to remove this glossy finish, the painted surface was lightly sanded with 600 grit sand paper. The rules established in Chapter 2 regarding system setup and grating size were maintained in this study.

4.3 Results and discussion

4.3.1 Woven composite with painted sections

A woven composite specimen was manufactured to use in the development of the test method. It was known that a balance must be found between transparency and opacity. For this reason, the testing area of this

woven composite was divided into four regions. Region 1 had no paint, Region 2 had a single coat of semi-transparent paint, Region 3 had two coats of semi-transparent paint, and Region 4 had the same opaque, matte, white paint as used in Chapter 2 of this thesis. The impact location was approximately at the intersection of these four regions. The different regions are shown in the image below with a grating projected onto the specimen. The area outlined with a dotted line is the portion of the specimen which is visible in Figures 4.2 and 4.3. The high speed camera was set to 7,000 frames/sec in this image since this is the frame rate which will be used during testing.

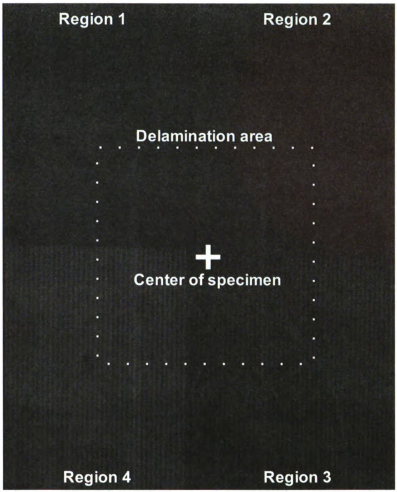

Figure 4.1. Woven composite specimen with four regions of different degrees of transparency. The dotted line shows the portion of the specimen which is visible in Figures 4.2 and 4.3.

One of the deformed images from the test on the above specimen is shown below outlining the delamination region to make it stand out. The impact point is noted as the + symbol in the image on the left. The impact point is at the center of the plate, however, the painted regions do not intersect exactly at the center of the plate.

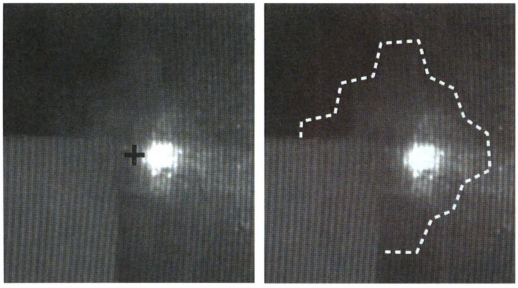

Figure 4.2. Typical image during delamination growth (left) and outline of the delamination shape (right). Only region outlined in Figure 4.1 is shown. The grid pattern of the delamination corresponds to the weaving geometry of the layers. The + indicates the impact point.

The symmetry of the delamination pattern in the image above could by utilized in future studies by painting one half of the specimen in matte white paint and leaving the other completely transparent. This would provide half of the specimen which was ideal for Projection Moiré and half that was ideal for identifying the delamination. It could then be assumed that the delamination was symmetric over this line since the lay up was orthotropic. Of course, it would be better not to have to make this assumption at all. For this reason, the method of simultaneously measuring the full field of both delamination and displacement through the use of semi-transparent paint was used in this thesis.

In order to show the delamination evolution and how Regions 1-3 performed relative to each other, a sequence of images during delamination growth are shown below.

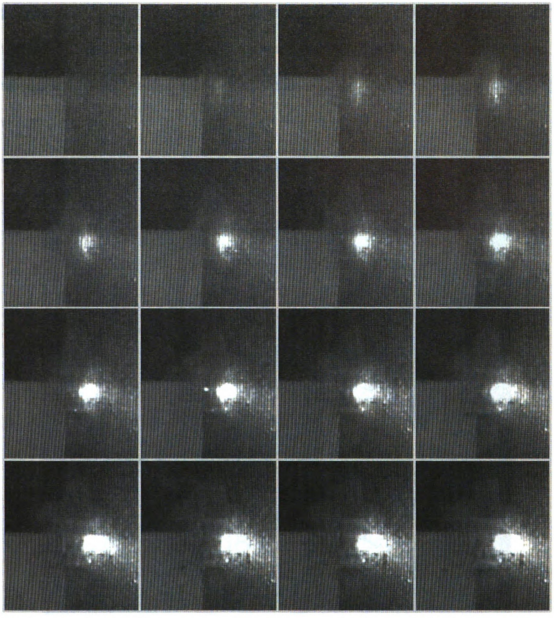

Figure 4.3. Delamination growth in the area outlined in Figure 4.1. Images are 0.14 ms apart.

The delamination is clearly visible in both Regions 1 and 2. It is still visible in Region 3, but to a lesser degree. Some of the difficulty in identifying the delamination area in Region 3, however, is due to the glare (an effect of the glossy paint) in that portion of the image. This effect is outlined with a solid line in the following figure. This problem was improved in subsequent testing by

lightly sanding the painted surface to remove the glossy effect of the paint. In the final five frames of the set of images shown above, fiber breakage can be seen. The region of fiber breakage is outlined with a dotted line for a sample image in the figure below.

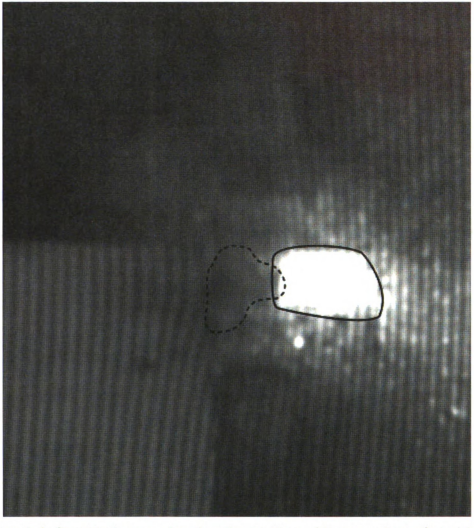

Figure 4.4. Sample image showing the portion of the specimen for which fiber breakage is developing. The fiber breakage is outlined with a dotted line. The glare is outlined with a solid line.

Once fiber breakage occurs, it is seen that the projected grating lines are no longer distinguishable in this portion of the specimen due to the blurring. The blurring could be caused by one of the following. First, the velocity of that portion

of the image could have been too high for the specified frame rate (7,000 frames/sec) of the camera to accurately capture. Since increased deformation causes the projected grating lines to move quickly, this could explain the blurring. Second, the out-of-plane displacement at that point could have been such that it was too far from the plane of focus for the camera. A higher camera frame rate could solve the first issue. The second issue could be solved by ensuring that the maximum displacement of the image was such that the camera would always be in focus.

Since the projected grating was visible on Regions 2-4, it was possible to calculate the out-of-plane displacement by the Projection Moiré method discussed in Chapter 2 of this thesis. The results are shown in the images below.

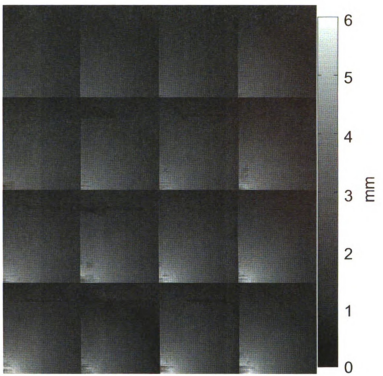

Figure 4.5. Projection Moiré results for Region 2.

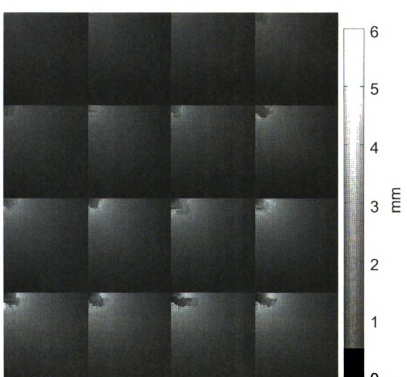

Figure 4.6. Projection Moiré results for Region 3.

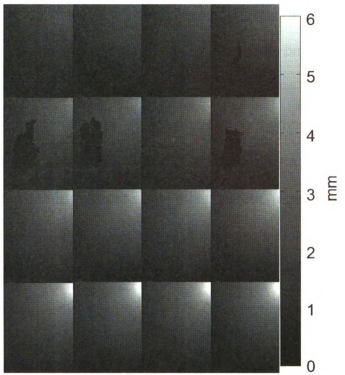

Figure 4.7. Projection Moiré results for Region 4.

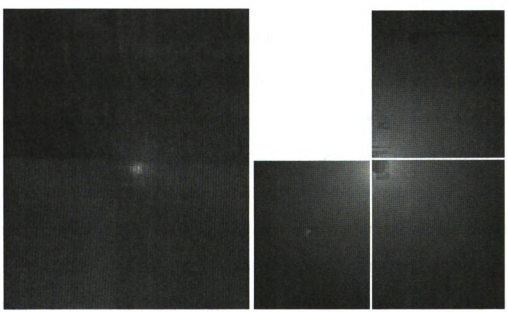

Figure 4.8. The unprocessed image of the specimen (left), and the Projection Moiré results for each region (right).

It is seen that the Projection Moiré results for early displacements work fine for all three regions. However, Regions 2 and 3 have problems for later frames, whereas Region 4 provides good results for all time. There are several factors that create problems. First, the glare near the loading point makes it difficult to identify the grating lines. Second, as fiber breakage develops, the grating lines are blurred. In order to solve this problem, future tests should be at an impact velocity such that fiber breakage is minimal or does not occur at all. Or, if fiber breakage does occur, develop techniques that allow for image recording at higher frame rates, such as 15,000 frames/sec as used in Chapter 2.

4.3.2 Cross-ply laminate

4.3.2.1 Cross-ply delamination

A $[0_4/90_4/0_4]$ translucent laminate with a thin layer of semi-transparent paint was impacted from a height of 320 mm. Only a thin coat was used in order to maximize the amount of delamination visible. Since delamination was the primary feature of this test to be measured, this was deemed acceptable. The Projection Moiré setup was implemented based on these images, but data processing revealed that not enough light was transmitted back to the camera to accurately calculate the out-of-plane displacement. The specimen still gave valuable insight into the delamination evolution within the specimen. In order to make the delamination more visible, the image contrast and brightness was adjusted. An example comparing the raw image to the adjusted image is shown below.

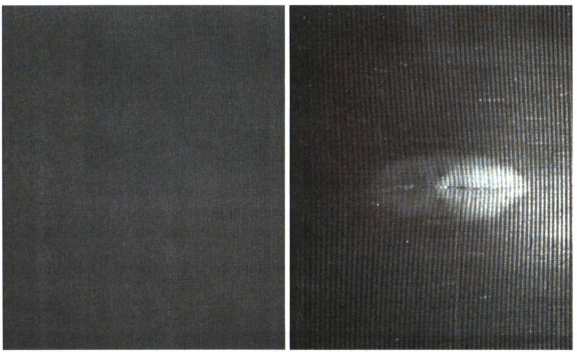

Figure 4.9. Modification of the contrast of the high speed camera image in order to make delamination more visible.

It is seen in the image that the delamination at each interface matched the peanut shape deformation found in the literature [4.3]. For the frame in the image above, an outline was drawn around each of these delamination regions. Solid lines indicate where the delamination is clearly seen. Dotted lines indicate an assumption made about the delamination shape based on the symmetry of the specimen and boundary conditions.

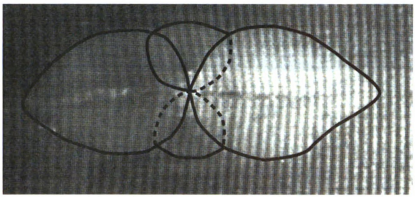

Figure 4.10. Outline of the delamination area which is visible in image (solid line) and the assumed delamination due to symmetry (dotted line).

The delamination region is shown for the period of delamination growth in the following set of image.

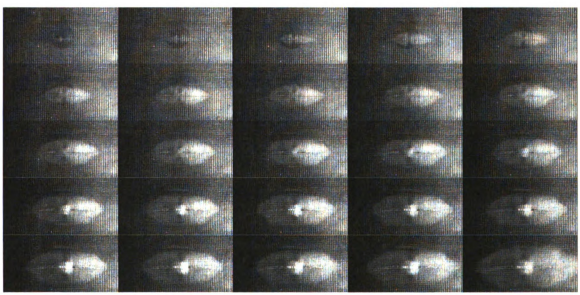

Figure 4.11. High speed camera images in the area of delamination for the period of delamination growth. Time between frames is 0.14 ms.

The corresponding force curve is shown in the figure below. The delamination area from the high speed camera is also shown.

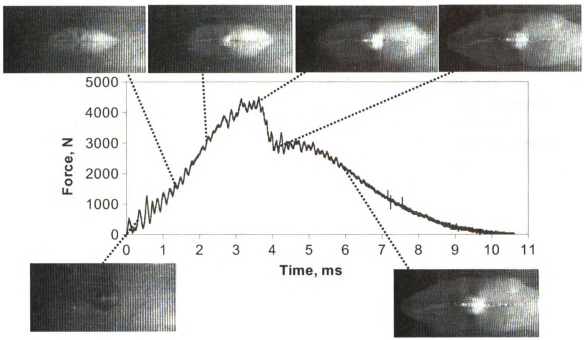

Figure 4.12. Comparison between the force history and the high speed camera images showing delamination.

4.3.2.2 Estimation of crack speed

Since the delamination growth between frames is visible, and the time step between frames is known, it is possible to calculate the average crack speed between two frames. Takeda was able to do this in a previous study [4.4], but the use of transparent composites should greatly simplify the process.

The crack is growing in many directions simultaneously, but the primary direction of growth is along the fiber direction of the bottom layer of the interface. For the rear layer, the crack speed has been calculated for each of the "arms" of the delamination. The average crack speed for both arms of the delamination was found to be 5.84 m/s.

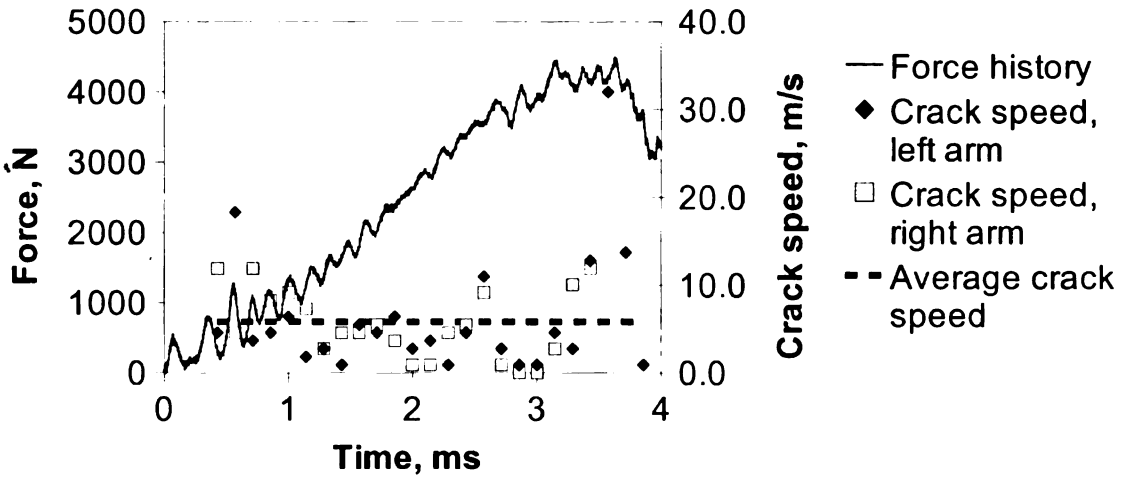

Figure 4.13 Comparison between the force history and the estimated crack speed of the primary direction of delamination.

The accuracy of the crack speed calculation is dependent on several factors. First, the camera resolution. Since it is only possible to determine if the delamination has propagated in discrete steps (pixels), it is not possible to determine the exact position of the crack tip. Second, the frame rate of the camera. Again, the time steps between frames are discrete values prescribed by the frame rate of the camera. This study identifies the pixel number at the crack tip and determines the crack speed by comparing this to the pixel number of the crack tip in the previous image. This means that each pixel of delamination growth between images corresponds to the following crack speed.

$$\frac{0.13\,mm}{pixel} * \frac{7{,}000}{sec} = 0.91\,m/s/pixel$$

For example, if the crack grew by 2 pixels, that would be a crack speed of 1.82 m/s. The calculation of the crack speed could be more accurately performed if a higher frame rate were used for the testing.

The length of each arm of delamination is plotted in the following image as a function of time. Note that, for the right arm, the delamination reached the edge of the imaged area before arresting. Shadows are cast on the specimen due to the thickness of the fixture, so the image edge is not the boundary edge. The delamination likely propagated further as was the case with the left arm. However, it is not possible to determine the arrest point from this test. In future testing, the experimental setup should be such that the entire delamination region is within the imaging area.

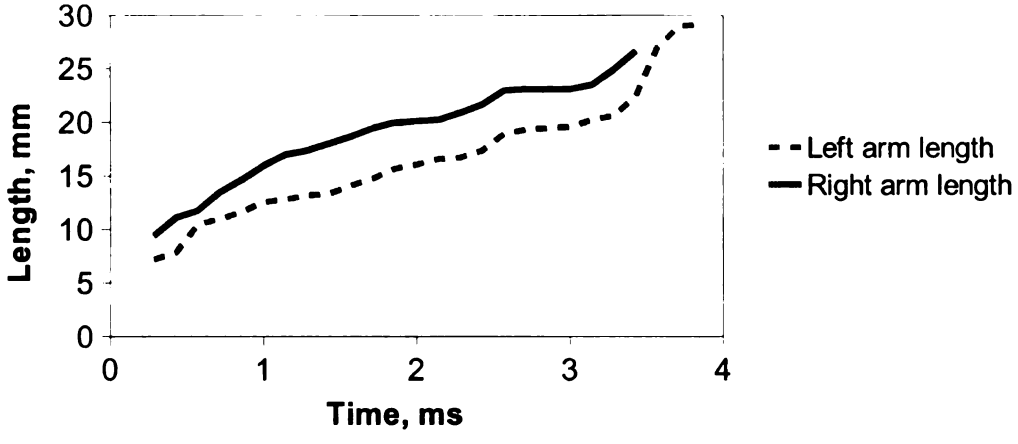

Figure 4.14. Length of each arm of the delamination in the rear layer of the laminate as a function of time.

There is a wide range of possible testing that could be performed in future work with this method. For example:

- Delamination resistance for different material configurations.
- The effect of the number of interfaces on the delamination initiation and propagation.
- The effect of strain rate on the delamination initiation and propagation

4.3.2.3 Projection Moiré with cross-ply laminate

In addition to the study of the delamination growth, the Projection Moiré method was applied to this specimen. The results for this analysis are summarized in the following figure. The frames in this image are 14 ms apart.

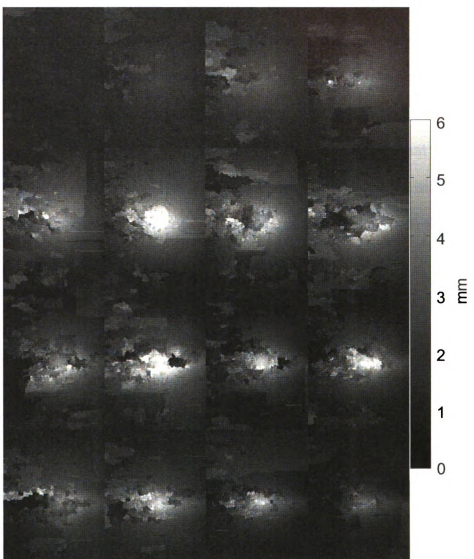

Figure 4.15. Projection Moiré results for the transparent cross-ply laminate. Time between frames is 0.57 ms.

Although the overall results of this image are not good, several useful observations can be made. First, The cross-ply laminate was initially more transparent than the woven composite from the initial study. This made it difficult to accurately reproduce the degree of translucency from the previous woven laminate. The same painting procedure as was used in Region 2 of the cross-ply laminate was implemented for the entire surface of the cross-ply laminate. However, the end result was more transparency for the laminate due to the difference in the transparency of the two plates prior to painting.

Second, It is seen that the primary portion of the image that fails to produce usable results is the left side of the image. This can be explained by taking into consideration the angle at which light is projected onto the specimen. The figure below demonstrates this.

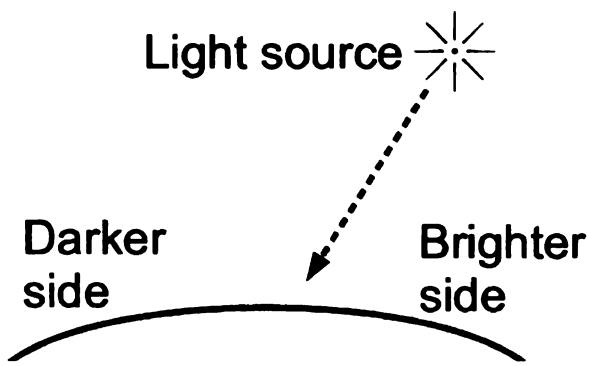

Figure 4.16. Schematic of how angle of light projection causes one side of the specimen to be darker than the other.

It is seen in this image that half of the deformed specimen will receive less light to reflect back to the camera than the other half. The darker half corresponds to the left side of the images in Figure 4.15 where the Projection Moiré results are the worst. In future testing, either more light must be projected onto the

specimen, a higher degree of light reflected back by decreasing the transparency of the specimen, or a camera with a higher sensitivity to light must be used.

Third, it is noted that the second region of the specimen that has a high degree of error is around the impact point. This corresponds to the increased velocity of this region as the fibers begin to break as discussed in the section about woven composites. This could be solved in future testing either by using a higher frame rate for the camera or by ensuring that the impact velocity was such that this phenomenon was avoided.

Being able to measure both the delamination and the deformation simultaneously presents an advantage. It allows for a correlation between the damage degree and the structural response. Since delamination changes the stiffness of the composite, it would be possible to objectively quantify the degree by comparing the out-of-plane displacement and the delamination size. Subsequent tests refined the method for achieving this.

4.3.3 Woven composite with half painted surface

In order to further explore the simultaneous implementation of translucent specimens and Projection Moiré measurements, additional cross-ply specimens were created. These new specimens were 2.25 mm thick consisting of woven cross-ply layers. The initial height for the impacting mass during the testing of these specimens was 150 mm. The frame rate of the high speed camera was held at 7,000 frames/sec as with the other tests in this chapter. The surface of one of these specimens was divided into two regions. One region was painted in the matte white paint used previously while the other region was left unpainted.

This provided half of the specimen with the ideal conditions for observing internal damage while the other region was the ideal condition for Projection Moiré measurements. Since the material and boundary conditions were symmetric across the boundary of these two regions, the behavior of the composite should be the same in each region. Symmetry could then be used to determine the full-field displacement and the full field internal damage. The specimen with the separate regions and the projected grating are shown in the following figure.

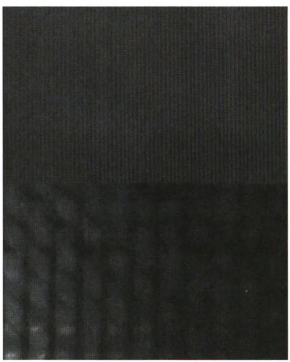

Figure 4.17. Woven translucent specimen with half of the rear surface painted white.

An additional light source was focused on the impacting surface of the specimen. The purpose of this light source was to increase the amount of light traveling through the translucent section of the plate. Since the Projection Morie section was fully opaque, the addition of this light source should not negatively effect the displacement calculation.

The out-of-plane displacement for the white section is plotted together with the damage progression in the figure below. The delamination in this specimen was less than for the previous specimens since the thickness of the composite was smaller. Due to the thin nature of the plate, fiber breakage took place earlier in the impact history and delamination arrested earlier. As the fiber breakage begins to occur, the quality of the Projection Moiré results in the area of fiber breakage decreases. This can be seen in the starting in the second image of the figure below. It is seen in the figure that both the delamination and the displacement can both be known through using this technique.

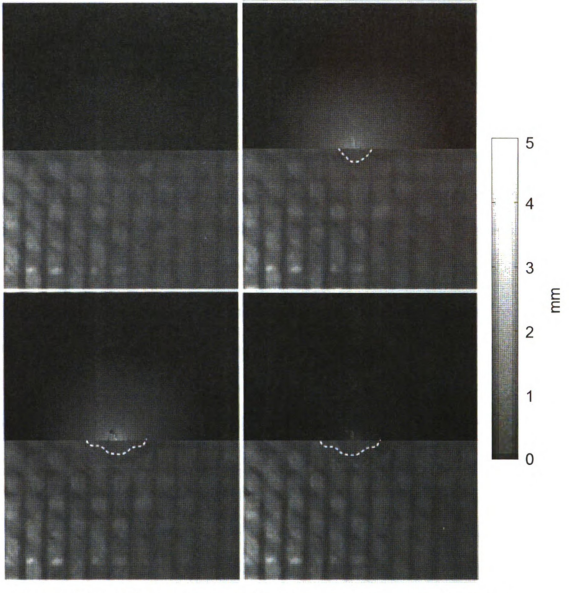

Figure 4.18. Projection Moire and delamination outlines for the woven composite with half of the surface painted white. Images are 2.86 ms apart.

4.3.4 Semi-transparent surface

There are conceivable testing conditions in which the boundaries or the material is not symmetric. The CL-L case from Chapter 3 of this thesis is an example such a case. Although a line of symmetry exists along the diagonal for

the boundary conditions, this is not a line of symmetry for the material. In order to perform a study in which both the damage and the displacement were desired for the full field, it would be necessary to be able to directly measure both quantities over the entires surface. It would not be useful to simply paint half of the specimen as was done in the previous section since symmetry would not allow one to make conclusions about the full-field. For this reason, it is desirable to further refine the method of measuring both simultaneously for the entire surface using semi-transparent paint.

Additional specimens like those in the above section were used to refine the method for identifying both internal damage and displacement for the full-field. One specimen was painted with two coats of the semi-transparent paint and lightly sanded to remove the glossy finish. The results of the Projection Moiré calculation are shown in the following image. It is seen int his figure that the overall trend in displacement is quite clear. There are some regions, however, that have noticeable errors. These errors appear in the darker side of the image and around the fiber breakage zone as previously identified. The number of regions in which errors occur, however, is drastically reduced in this test as compared with the cross-ply laminate.

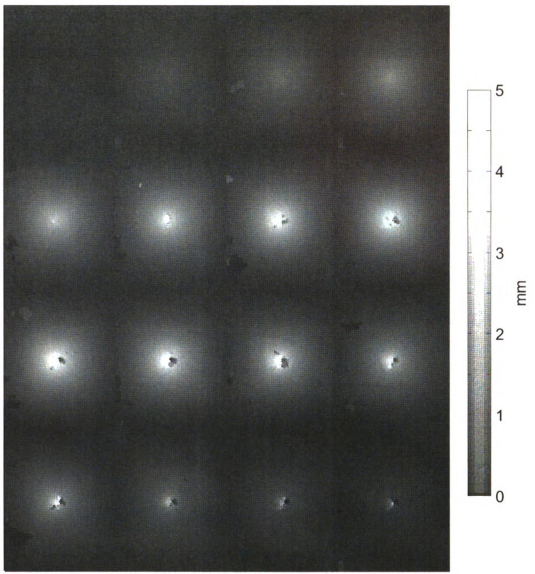

Figure 4.19. Projection Moire results for the translucent composite with two coats of semi-transparent paint.

The next step in analyzing this specimen is to determine if the growth in delamination can be seen through the painted surface. The following images show the evolution of the delamination. In this image, the brightness and contrast of the image were adjusted to make the delamination pattern visible in the document. Although there are portions of the delamination which are clearly visible, other portions of the specimen are more difficult to observe. Still, an

outline of the delamination can be drawn with a reasonable degree of confidence. Dotted lines are used instead of solid lines to indicate a degree of uncertainty in identifying the delamination area.

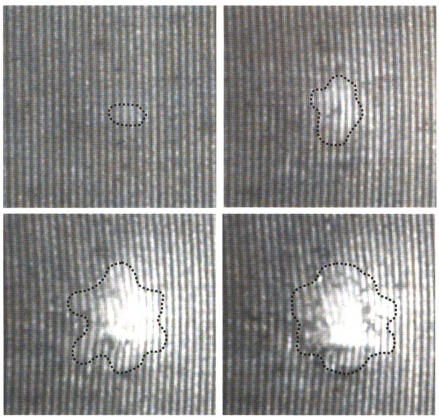

Figure 4.20. Delamination growth in the woven composite with two coats of semi transparent paint. Time steps between the images was 1.43 ms.

Since it was desired to obtain the delamination area with a higher degree of certainty, a specimen was tested in which only one coat of semi-transparent paint was applied to the surface. The DWIT setup parameters were the same as those as for the previous specimen. Since there was less paint on the surface, less light was reflected back to the camera. Therefor, it was expected that the Projection Moiré results would be of a slightly lower quality that those for the specimen with two coats.

The following image shows the out-of-plane displacement for the specimen with one coat of semi-transparent paint.

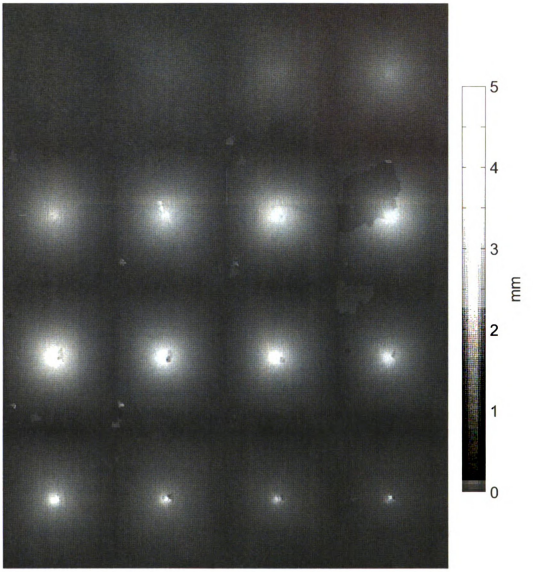

Figure 4.21. Projection Moiré results for the woven specimen with one coat of semi-transparent paint. Images are 0.57 ms apart.

It is seen that there are slightly more errors due to the illumination intensity than there were for the case of the specimen with two coats of semi-transparent paint. However, the overall results are quite good. The trend in each individual image is clear, and the trend with respect to time matches the expected results.

Again, the region where delamination took place was inspected to see the growth with time.

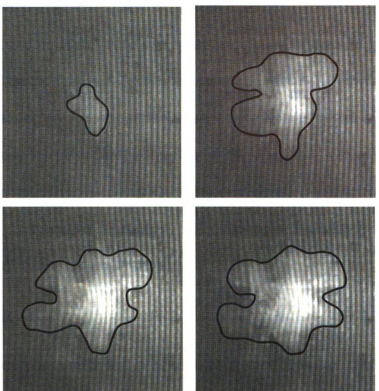

Figure 4.22. Delamination growth in the woven composite with one coat of semi transparent paint. Time steps between the images was 1.43 ms.

4.4 Conclusions

It is seen from this study that the observation of delamination growth is greatly enhanced through the use of translucent composite materials. With this approach, it is possible to determine not only the final delamination area, but the progress of delamination throughout the impact event.

Additionally, it is possible to perform Projection Moiré measurements at the same time as observing the internal damage. There are two techniques which can be used. First, if the boundary conditions and material are both

symmetric, half of the specimen can be painted white while the remaining half is left uncoated. If the setup is symmetric, the behavior can be mirrored over the boundary between the painted and unpainted surface.

The second approach is to use a semi-transparent paint to coat the entire rear surface of the specimen. Using this technique requires some effort to determine an acceptable compromise between transparency and translucency. If the specimen is too transparent, the Projection Moiré measurements will not work, and if the specimen is too opaque, the delamination will not be visible. If an acceptable compromise is reached, both the displacement and internal damage can be measured accurately.

4.5 Future work

It has been demonstrated here that the internal damage of a specimen during an impact event can be measured with the use of translucent composites. Since one of the primary concerns when comparing different composite structures is their resistance to delamination, it would be beneficial to compare different composites (stacking sequence, weave geometry, etc.) by measuring the delamination with respect to time.

It was seen during the use of semi-transparent paint that, while the overall Projection Moiré results were good, there was still some portions of the specimen which contained errors. In order to further refine the method, these errors should be eliminated. The reason for these errors was primarily due to the darkness of the image. There are several factors which could improve these results. First, increase the amount of light reflected from the specimen back to the camera. A

considerable amount of refinement has already been presented for this factor in this thesis. The second contributing factor is the amount of light provided by the light source. Increasing the amount of projected light would increase the brightness of the recorded image. This could be done by optimizing the grating projection system. Several of the components could be refined including the light source, lens selection, and component location. The third factor is the light sensitivity of the camera. High speed camera light sensitivity decreases with increasing frame rate due to the decrease in exposure time. As high speed camera technology continues to improve, this problem should be alleviated.

4.6 References

[4.1] Takeda, N, Sierakowski, RL, Ross, CA, and Malvern, LE, "Delamination-crack propagation in ballistically impacted glass/epoxy composite laminates," 1982, *Experimental Mechanics*, Vol. 22, 19-25.

[4.2] Dhyani, A, "VARTM Process With Some Modifications," Master's Thesis, Michigan State University, East Lansing, MI, 2008.

[4.3] Liu, D. "Impact-Induced Delamination - A View of Bending Stiffness Mismatch," *Journal of Composite Materials*, Vol. 22, 1988, pp. 674-692.

[4.4] Rosario, K, "Quasi-three-dimensional woven composites," Master's Thesis, Michigan State University, East Lansing, MI, 2008.

Chapter 5: Conclusions and future work

5.1 Conclusions

5.1.1 Impact testing with Projection Moiré

It has been established in this study that Projection Moiré is an acceptable measurement tool for measuring displacement during plate impact testing. The work done by other researchers has streamlined its implementation, and allows for an efficient measurement system.

The full-field displacement provided by the rear surface measurements give a comprehensive evaluation of the specimen. Through observation of these results, it is possible to observe the initiation and growth of major delamination. This was due to the fact that delamination causes a localized degradation of the bending stiffness, and thus a discontinuity in the slope of displacement. The observations are enhanced by plotting the displacement profile along lines through the impact point. Major delamination is distinguished by a protruded region which forms during the loading portion of the force curve, and grows to its maximum value at the peak force.

The results from the Projection Moiré measurement of the rear surface were compared to the load cell measurements of a single point on the impact surface. The results were quite close to each other considering that the measurements were taken on opposite surfaces in the structure. Since it was known that indentation on the impact surface would cause the results from each

surface to be distinct, it was concluded that both techniques give an adequate measurement of the structure's response.

5.1.2 Material properties from impact testing

The method of using mode shapes as virtual fields was found to perform better than the method of manually selecting functions to use as virtual fields. Since the mode shapes provide independent virtual displacements, they provide useful fields to use in application.

It was found that the CL-L set of boundary conditions provided the best results for applying the Virtual Fields Method for the current loading scenario. The selection of this case was a result of finding a balance between the following contributing factors.

1. The best results are obtained when the boundary conditions are less restrictive. For example, better results are obtained with simply supported than with clamped boundary conditions.
2. The selected set of boundary conditions must be selected such that each bending stiffness influences the plate response significantly enough. For example, The CL-L configuration performs better than the CL-4 configuration.
3. The selected set of boundary conditions must be practical for experimental implementation. For example, clamped edges can be implemented simply and consistently in experiments whereas simply supported edges cannot.

Although the numerical study was based on static loading, it is thought that the configuration should also be the best configuration for dynamic loading. This conclusion is due to the fact

5.1.3 Translucent composites for studying damage progression

It is seen from this study that the observation of delamination growth is greatly enhanced through the use of translucent composite materials. With this approach, it is possible to determine not only the final delamination area, but the progress of delamination throughout the impact event.

Additionally, it is possible to perform Projection Moiré measurements at the same time as observing the internal damage. There are two techniques which can be used. First, if the boundary conditions and material are both symmetric, half of the specimen can be painted white while the remaining half is left uncoated. If the setup is symmetric, the behavior can be mirrored over the boundary between the painted and unpainted surface.

The second approach is to use a semi-transparent paint to coat the entire rear surface of the specimen. Using this techinque requires some effort to determine an acceptable compromise between transparency and translucency. If the specimen is too transparent, the Projection Moiré measurements will not work, and if the specimen is too opaque, the delamination will not be visible. If an acceptable compromise is reached, both the displacement and internal damage can be measured accurately.

5.2 Future work

5.2.1 Impact testing with Projection Moiré

The addition of the Projection Moiré setup to the impact of composite plates provides a valuable means for quantifying the rear surface specimen response. Past studies [1.4] have shown the importance of the rear layer in the energy absorbing properties of a composite plate. Future work should use this setup to quantify the performance of different structures by measuring the full-field displacement. Such a study should provide a more thorough understanding of the individual plate's performance and thus a better comparison of alternative materials.

It has been shown in this chapter that the measurements by the load cell on the impact surface and the measurements by Projection Moiré of the rear surface both give reasonable results. Differences between the displacements has been primarily attributed to the indentation on the impact surface. Indentation tests were conducted on different specimens and a different set of boundary conditions than was used in the impact tests presented in this chapter, however. In order to more fully compare the impact and rear surfaces, indentation tests should be performed using the same specimen as used in this chapter and with the same boundary conditions.

5.2.2 Material properties from impact testing

The methodology presented in this chapter for implementing the Virtual Fields Method needs further refinement. It was seen that the curvature fields

contained a large amount of noise. Further study needs to be conducted to reduce this. Future work should focus on reducing the noise in the displacement data as well as on alternative techniques to smooth the data before differentiation. In addition to the data processing, the fixture design needs to be refined. Presently, the entire specimen is not illuminated by the grating projection system. The fixture needs to be refined in order to obtain the optimum size and location of the mirrors for the prescribed projection angle.

In order to implement the Virtual Fields Method for impact testing, a set of intermediate steps has been proposed in this thesis. Steps include static testing, quasi-static simulation/testing, and dynamic simulation/testing. If this procedure is followed, each source of error should be eliminated systematically. In addition to refining the methodology, final result would allow for the comparison of material properties at various strain rates.

5.2.3 Translucent composites for studying damage progression

It has been demonstrated here that the internal damage of a specimen during an impact event can be measured with the use of translucent composites. Since one of the primary concerns when comparing different composite structures is their resistance to delamination, it would be beneficial to compare different composites (stacking sequence, weave geometry, etc.) by measuring the delamination with respect to time.

It was seen during the use of semi-transparent paint that, while the overall Projection Moiré results were good, there was still some portions of the specimen which contained errors. In order to further refine the method, these errors should

be eliminated. The reason for these errors was primarily due to the darkness of the image. There are several factors which could improve these results. First, increase the amount of light reflected from the specimen back to the camera. A considerable amount of refinement has already been presented for this factor in this thesis. The second contributing factor is the amount of light provided by the light source. Increasing the amount of projected light would increase the brightness of the recorded image. This could be done by optimizing the grating projection system. Several of the components could be refined including the light source, lens selection, and component location. The third factor is the light sensitivity of the camera. High speed camera light sensitivity decreases with increasing frame rate due to the decrease in exposure time. As high speed camera technology continues to improve, this problem should be alleviated.

Appendix A: Dynamic indentation behavior

Abstract

Static indentation laws have been established in the literature. It is possible, however, that the properties governing the material's behavior are different for dynamic loading cases. In order to fully characterize a material, it is necessary to establish a dynamic indentation law. The present study establishes such a law. It was found that the form of the governing equation was the same as for static loading, however, the fitting constants were different. In addition to identifying dynamic behavior, indentation testing reveals information concerning the damage process during impact tests. Since indentation is one of the damage modes present in plate impact testing, quantifying its contribution to the damage process would provide insight into the process as a whole. In the present study, the indentation law and testing results were used to obtain the amount of energy which was absorbed by the material due to the indentation process.

A.1 Introduction

Work with concerning the energy absorbing properties of composite materials has been a subject of investigation by several researchers. Liu [A.1] showed which damage modes were important to the energy absorption and the time period for which each mode was dominant. It was shown that indentation indentation was dominant at early stages of the impact event.

The indentation law for static loading is well established. Yang and Sun [A.2] showed that a power law relationship with an exponent of n = 1.5 accurately

modeled the force-indentation relationship for glass/epoxy laminates under static loading. This relationship was valid only for the loading process.

$$F = K\alpha^{n} \tag{A.1}$$

In this equation, F is the force, α is the indentation, and K is a fitting constant. Tan and Sun [A.3] presented an equation to predict the value of K based on material properties and the system configuration.

$$K = \frac{4}{3}\frac{R^{1/2}}{\frac{1-\nu_i^2}{E_i}+\frac{1}{E_{22}}} \tag{A.2}$$

In this equation, R is the radius of the impactor, ν_i and E_i are Poisson's Ratio and Young's Modulus of the impactor, respectively, and E_{22} is the transverse Young's Modulus of the composite plate. The indentation law resulting from these equations has been widely used in dynamic studies for years although it has only been proven valid for static loading rates. Lee and Liu [A.4] showed in their experiments that there is a strain rate effect in the force-indentation relationship, thus proving that the static indentation properties cannot be used for dynamic analysis.

A.2 Methods

A.2.1 Measurement of maximum indentation

Since it is not feasible to measure the displacement history during the impact event, the maximum indentation was recorded by the use of marker paint

on the specimen as demonstrated by Lee and Liu [A.4]. A mark was left on the impactor after impact had occurred. The maximum displacement can be calculated from the radius of paint left on the hemispheric impactor. In the following equation, α is the amount of indentation, d is the diameter of marker paint measured on the impactor, and R is the radius of the impactor.

$$\alpha = R\left(1 - \sqrt{1 - \left(\frac{d}{2R}\right)^2}\right) \tag{A.3}$$

In order for this measurement technique to be valid, the impactor head must be hemispheric in shape. The impactor is shown in the following figure. It is seen that the shape can be considered the correct shape.

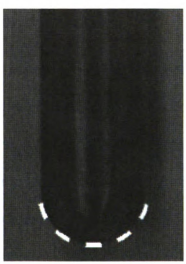

Figure A.1. Image of the impactor (left) and definition of geometry symbols (right).

An image of the specimen after impact is shown in the following figure. It is seen how the paint transfers from the specimen surface to the impactor in the indentation zone. For consistency, the same indentation measurement was used in dynamic and static indentation tests.

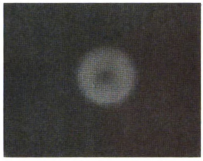

Figure A.2. Image of the specimen after indentation.

The specimen used was a 25.4 mm (1 in) thick cross-ply glass/epoxy laminate manufactured from 3M. Each indentation location was greater than or equal to twice the impact diameter from any previous impact location and the edge of the specimen.

A.2.2 Dynamic indentation

The device used in this study to create the dynamic loading was the Dynatup drop-weight impact tester, model 8250, as discussed in Chapter 2 of this thesis. The only difference in this case is that the standard fixture was replaced by a 76 mm (3 inch) thick steel block. This was to ensure that the rear support of the specimen was completely rigid. In order to determine the effect of velocity on the indentation relationship, several impact velocities were chosen for the study. For each velocity, a range of impacting masses was used. The largest weight used for a given velocity was dictated by the capacity of the load cell.

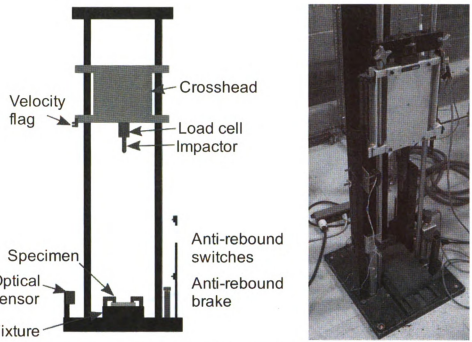

Figure A.3. Schematic of the DWIT machine (left) and the actual device (right).

A.2.3 Static indentation

In order to ensure consistency between the static and dynamic measurements, it was desired that the both set of tests be conducted on the same machine with the same measurement devices. In order to achieve this, the DWIT was modified to allow for static loading. A frame was build around the crosshead, as shown in the following figure. A hydraulic press was then placed between the frame and the crosshead to apply the load. Springs were attached to prevent the crosshead from loading the specimen prematurely. Indentation measurements were made with the same method as used in dynamic testing.

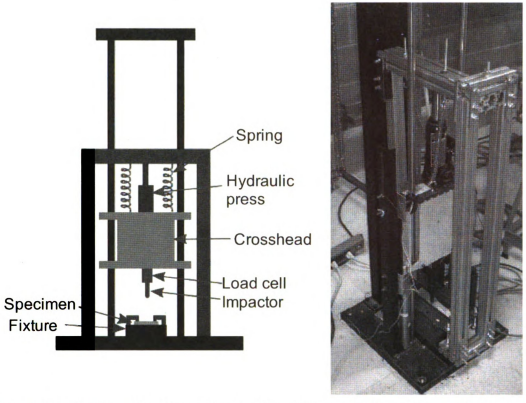

Figure A.4. Schematic of the static setup (left) and picture of the actual device (right).

A.3 Results and discussion

The force-indentation relationship from the dynamic indentation tests was plotted along with static indentation data from Lee and Liu's study [A.4]. The static data was updated to reflect a more accurate system calibration. A power law curve was fit to both the static and the dynamic data.

As expected, a strain rate effect was seen in the data. Power law relationships were fit to the data. Two plots are presented in below. For Figure A.5, the exponent, n, of Equation (A.1) was held constant at 1.5. In Figure A.6, n was allowed to vary as part of the fitting process. In each plot, curves were fit to

each data set individually as well as a curve fit to all three dynamic data sets together. The constants for each fit curve are presented in Table A.1.

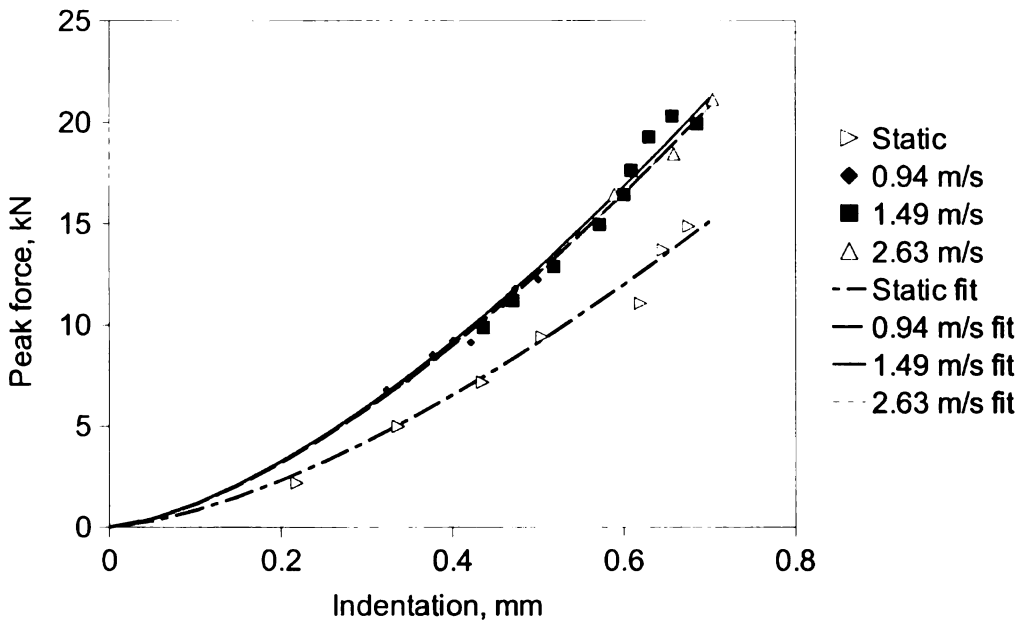

Figure A.5. Indentation results with power law fitted curves (n = 1.5).

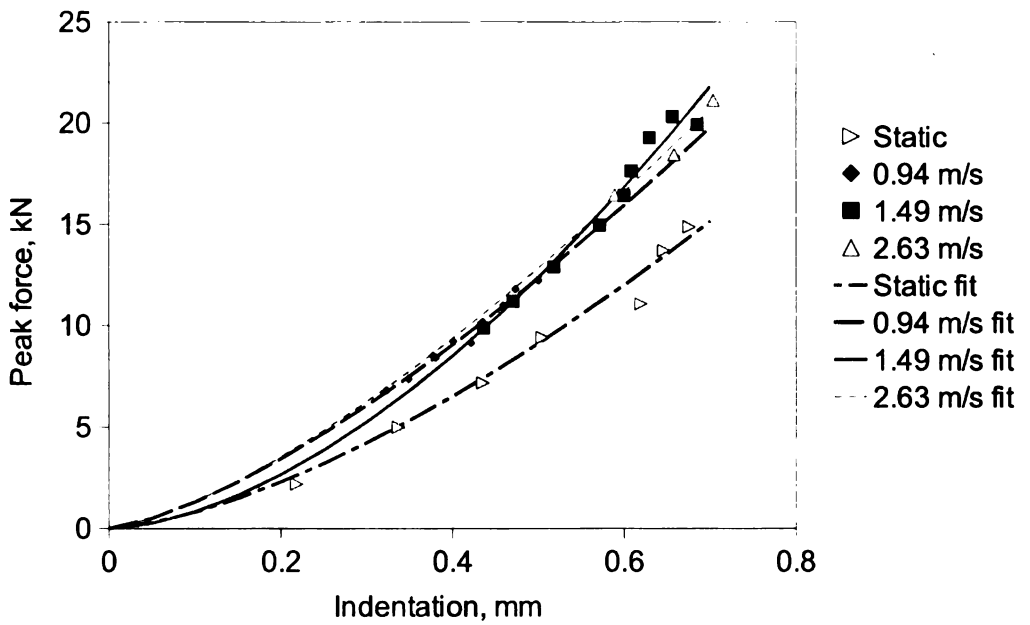

Figure A.6. Indentation results with power law fitted curves (n is variable).

It was found that the correlation coefficients for each of the curves were quite high. The fitting curves are compared graphically in Figure A.7. Since all of the dynamic curves with an exponent of n = 1.5 were nearly overlapping; only the curve fit to all of the data was used in Figure A.7. This was done to make the plot easier to read.

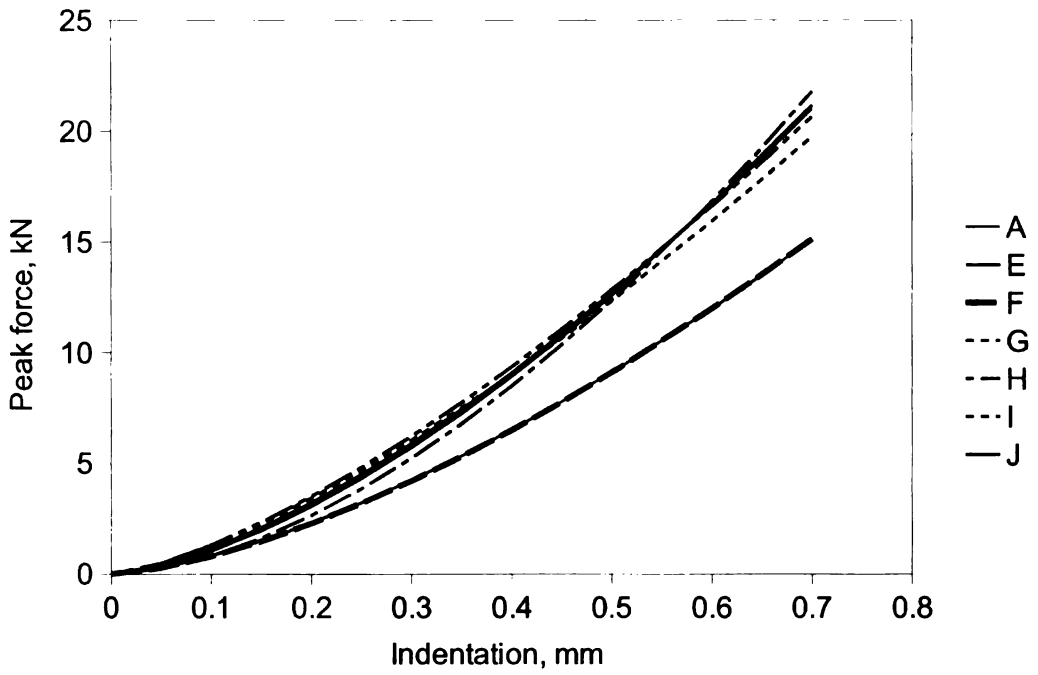

Figure A.7. Comparison between the fitting curves shown in Figures A.5 and A.6.

Table A.1. Fitting constants for the power law curves fit to the indentation data

Test	Static	0.94 m/s	1.49 m/s	2.63 m/s	All dynamic
ID	A	B	C	D	E
K	25.8	35.5	36.2	35.5	35.9
n	1.5	1.5	1.5	1.5	1.5
r^2	0.97	0.98	0.95	0.96	0.99
ID	F	G	H	I	J
K	25.9	32.5	39.7	34.2	36.7
n	1.51	1.40	1.68	1.41	1.54
r^2	0.97	0.98	0.97	0.96	0.99

The high degree of correlation between the fitted lines and the indentation data justifies the use of the power law in modeling the material behavior. The correlation coefficient for each of the fitting curves is quite high, as seen in Table A.1. Since the r^2 values for the case of n = 1.5 are so close to those for when n is allowed to vary, the power law with the 1.5 exponent can be accepted as the appropriate indentation law for dynamic studies.

It is seen that there is substantial deviation from the static indentation law for impact loading rates. There is not noticeable variation within the impact data for the range of impact loading rates applied in this study, however. Within this range, strain rate effects can be assumed negligible. The use of the static indentation law for dynamic analysis would be in error. If a dynamic study is to be conducted, the researcher must first establish the dynamic indentation law to be used.

With the force-indentation relationship known, it is now possible to calculate the amount of energy absorbed during the indentation process. Since absorbed energy is simply the integral of force with respect to displacement, the energy of the loading process can be calculated as

$$U=\int_a^b k\alpha^n d\alpha=\frac{k}{n+1}\left(b^{n+1}-a^{n+1}\right) \tag{A.4}$$

where K is determined from the appropriate dynamic indentation law. This calculation is made possible by the assumption that the load cell is rigid. For the case of n = 1.5, the loading energy is described as follows.

$$U=\int_a^b k\alpha^{1.5} d\alpha=0.4k\left(b^{1.5}-a^{1.5}\right) \tag{A.5}$$

A.4 Conclusions

The indentation law is dependent on the loading rate of the system. Use of static indentation laws cannot be considered valid for analysis of dynamic events. As a result, using Equation (A.2) to predict the value of K would provide an incorrect value for a dynamic case. A study must be performed for a given configuration in order to determine the appropriate indentation law coefficient to be used. For small changes in impact velocity, there is not a noticeable change in the indentation law, however. If the dynamic indentation law is known for a material, it is possible to calculate the amount of energy absorbed by the indentation loading process.

A.5 Future work

The present work has established the dynamic indentation behavior for a range of velocities from 0.94 – 2.63 m/s. It was observed that, within this range, the response did not change significantly. In order to better understand the effect of strain-rate on the material's response, future work should investigate a larger range of impact velocities.

It is now known how specimen geometry such as stacking sequence, weaving geometry, and thickness effect the dynamic indentation response. Future work should investigate these factors in order to know more fully how the indentation law can be applied.

Additionally, only the peak indentation could be measured in this test. In order to have a more complete characterization of the indentation response, the complete loading and unloading history is required. Future work should include a study which obtains each of these quantities.

A.6 References

[A.1] Liu, D., "Characterization of Impact Properties and Damage Process of Glass/Epoxy Composite Laminates," Journal of Composite Materials, Vol. 38, 2004, pp. 1425, 1442.

[A.2] Yang, S.H. and Sun, C.T., "Indentation law for composite laminates," Composite Materials: Testing & Design (6th Conference), ASTM STP 787, Daniel, IM, Philidelphia, PA: American Society for Testing and Materials, 1981, 425-449.

[A.3] Tan, T.M., and Sun, C.T., "Use of Statical Indentation Laws on the Impact Analysis of Composite Laminated Plates," Journal of Applied Mechanics, Vol. 52, 1985, pp. 6, 12.

[A.4] Lee, C.-Y., and Liu, D., "Effect of impact velocity on the indentation of thick composite laminate," Experimental Techniques. 2008, pp. 1, 6.

Appendix B: Drop-weight impact tester calibration

B.1 DWIT data acquisition calibration

The data acquisition system for the force measurement consists of the following components: load cell, amplifier, signal conditioning unit, input impedance, computer with data acquisition card, and digital oscilloscope software. The system is shown schematically below. In this system, the Signal conditioning (ie. amplification, excitation) was performed by the Ectron 778 unit. The recorded data has units of volts and will be multiplied by a calibration factor to obtain force. This procedure will be discussed later.

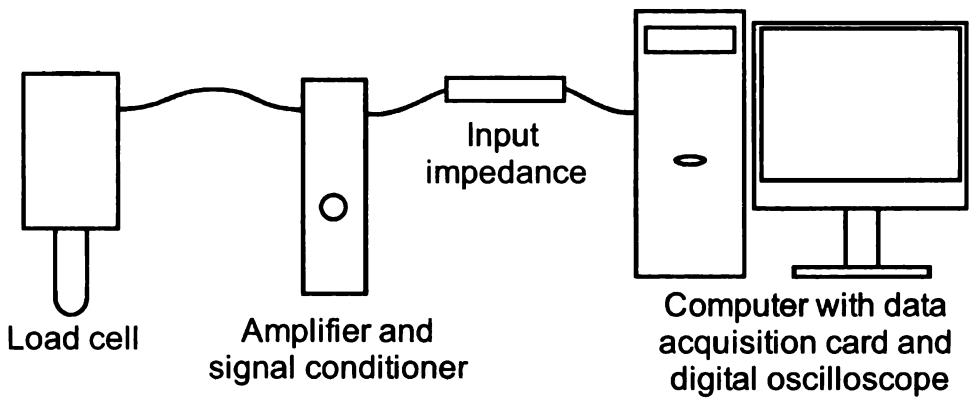

Figure B.1. Schematic of the data acquisition system.

In order to be able to trust the results from the Dynatup machine, it is important that the data acquisition system be calibrated prior to each study performed. The first step in calibrating the system is to verify that each component is in proper working condition. The simplest components to check are the cables. A multi-meter was used to check the resistance between pins – they should be less than 1 Ω each. It was determined that all of the resistances were in the expected range.

It is known that the load cell should be provided with an excitation of 5V. The voltage across the excitation of the amplifier was measured and determined to be 5 V exactly, so no adjustments were needed. This voltage was measured statically, however. It is possible that there is some fluctuation in the voltage when the Wheatstone bridge is under dynamic loading. In order to verify the results obtained in the setup above, excitation was supplied by a power supply instead of the Ectron unit. The power supply was of a much better quality, so the results could be more readily trusted. It was found that the results from the two excitation sources matched quite well. Therefor, the Ectron unit can be trusted to provide the correct excitation.

In order to ensure that gain of the amplifier was being applied correctly and that the measurement in the digital oscilloscope was correct, a series of known voltages were applied to the input of the Ectron unit. The measured voltage on digital oscilloscope was found to be the correct amplification of the supplied signal, so the measurement system was operating correctly.

The data acquisition card's clock was checked by comparing it to a satellite-synchronized clock over the course of 30 minutes. Data acquisition was initiated and the time of initiation was recorded according to the satellite clock. The time history recorded by the data acquisition card was found to vary less than 1% from the satellite clock, so the error was deemed acceptable.

B.2 Load cell calibration

The load cell was calibrated by placing a series of static weights onto the specimen. The measurement range of the load cell was 22 kN (5000 lbs). Since

it would not be safe to apply this high of a loading, loads of 0 - 3.9 kN (0 - 877 lbs) were applied incrementally. The maximum force was determined by the amount of dead weights available. At each increase of load, the output voltage was recorded on the oscilloscope. A gain of 10 was used during the calibration since that is the gain that would be used in the impact testing. The calibration factor to convert the unamplified voltage to units of force was found to be 40.7 kN/V (9156 lb/V).